

# Phase Transitions in an Expanding Universe: Stochastic Gravitational Waves in Standard and Non-Standard Histories

Huai-Ke Guo<sup>a</sup> Kuver Sinha<sup>a</sup> Daniel Vagie<sup>a</sup> Graham White<sup>b</sup>

<sup>a</sup>Department of Physics and Astronomy, University of Oklahoma, Norman, OK 73019, USA

<sup>b</sup>TRIUMF Theory Group, 4004 Wesbrook Mall, Vancouver, B.C. V6T2A3, Canada

E-mail: [ghk@ou.edu](mailto:ghk@ou.edu), [kuver.sinha@ou.edu](mailto:kuver.sinha@ou.edu), [Daniel.d.vagie-1@ou.edu](mailto:Daniel.d.vagie-1@ou.edu), [gwhite@triumf.ca](mailto:gwhite@triumf.ca)

**Abstract.** We undertake a careful analysis of stochastic gravitational wave production from cosmological phase transitions in an expanding universe, studying both a standard radiation as well as a matter dominated history. We analyze in detail the dynamics of the phase transition, including the false vacuum fraction, bubble lifetime distribution, bubble number density, mean bubble separation, etc., for an expanding universe. We also study the full set of differential equations governing the evolution of plasma and the scalar field during the phase transition and generalize results obtained in Minkowski spacetime. In particular, we generalize the sound shell model to the expanding universe and determine the velocity field power spectrum. This ultimately provides an accurate calculation of the gravitational wave spectrum seen today for the dominant source of sound waves. For the amplitude of the gravitational wave spectrum visible today, we find a suppression factor arising from the finite lifetime of the sound waves and compare with the commonly used result in the literature, which corresponds to the asymptotic value of our suppression factor. We point out that the asymptotic value is only applicable for a very long lifetime of the sound waves, which is highly unlikely due to the onset of shocks, turbulence and other damping processes. We also point out that features of the gravitational wave spectral form may hold out the tantalizing possibility of distinguishing between different expansion histories using phase transitions.

---

## Contents

<b>1</b>	<b>Introduction</b>	<b>1</b>
<b>2</b>	<b>Theoretical Framework</b>	<b>4</b>
2.1	Gravitational Waves	4
2.2	Unequal Time Correlator of the Fluid Stress Energy Tensor	6
<b>3</b>	<b>Dynamics of the Phase Transition</b>	<b>8</b>
3.1	Bubble Nucleation Rate	8
3.2	False Vacuum Fraction	10
3.3	Unbroken Bubble Wall Area	12
3.4	Bubble Lifetime Distribution	13
3.5	Bubble Number Density	15
3.6	Relation between $\beta$ and Mean Bubble Separation ( $R_*$ )	17
<b>4</b>	<b>Fluid Velocity Field and Power Spectrum</b>	<b>19</b>
4.1	Fluid and Field Equations	20
4.2	Velocity Profile around a Single Bubble	22
4.2.1	Inside the Bubble	22
4.2.2	Outside the Bubble	23
4.2.3	Matching at Bubble Wall	24
4.3	Velocity Field in the Sound Shell Model	26
4.4	Velocity Power Spectrum	28
<b>5</b>	<b>Gravitational Wave Power Spectrum</b>	<b>30</b>
5.1	Solutions in Radiation and Matter Domination	31
5.2	Gravitational Wave Power Spectrum	33
5.3	Lifetime of the Source	38
5.4	Spectrum Today	39
<b>6</b>	<b>Summary</b>	<b>42</b>
<b>7</b>	<b>Acknowledgments</b>	<b>42</b>
<b>A</b>	<b>The Example Effective Potential</b>	<b>42</b>
<b>B</b>	<b>The Previously Derived Effective Lifetime of the Source</b>	<b>44</b>

---

## 1 Introduction

Primordial stochastic gravitational waves from first order cosmological phase transitions have become a new cosmic frontier to probe particle physics beyond the standard model [1–6]. Alongside extensive studies on the theory side, direct searches for stochastic gravitational waves at LIGO and Virgo have

also been performed using their O1 and O2 data sets [7, 8]. Perhaps even more significantly, space-based detectors which can probe lower frequencies coming from an electroweak scale phase transition are poised to come online within the next decade or so [9–21].<sup>1</sup>

Precise calculations of the gravitational wave power spectrum are required to have any hope of inferring parameters of the underlying particle physics model. There have been significant advances in this direction in recent years. In particular, it is now generally accepted that the dominant source for gravitational wave production in a thermal plasma are the sound waves [38], although a more precise understanding of the onset of the turbulence is still needed to settle this issue. For the acoustic production of gravitational waves, many large scale numerical simulations have been performed [39, 40], with the result that standard spectral formulae are now available for general use. These results have also been understood reasonably well for relatively weak transitions, through the theoretical modeling of the hydrodynamics [41] and with the recently proposed sound shell model [42, 43].

The first major goal of this paper is to undertake a careful analysis of the gravitational wave power spectrum in a generic expanding universe. This is necessary, since the standard result for the spectrum is obtained in Minkowski spacetime where the effect of the expansion of the universe is neglected. The spectrum depends on the lifetime of the source (the sound waves); it has been shown in [39], based on simple rescaling properties of the fluid, that the effective lifetime of the source is a Hubble time, such that  $H_* \tau_{\text{sh}} \approx 1$ , where  $H_*$  is the Hubble parameter at the phase transition and  $\tau_{\text{sh}}$  the lifetime of the source. We note, however, that many approximations were used in arriving at this result, some of which may bear deeper scrutiny. We present a comprehensive and very careful analysis of the spectrum, clarifying subtle issues when the calculation is generalized from Minkowski spacetime to an expanding universe, and ultimately providing an accurate spectrum in a standard radiation dominated universe and in other expansion scenarios. We perform a detailed calculation of the nucleation and growth of bubbles in an expanding background, including tracking the shrinking volume available for new bubbles to nucleate in as well as the total area of uncollided walls. Both are needed for an accurate understanding of how the volume fraction and mean bubble separation evolve throughout the phase transition. We then derive and solve the equations governing the evolution of the fluid velocity field in an expanding Universe and then proceed to a derivation of the spectrum for different expansion scenarios.

The second major goal of this paper is encapsulated in the title: after having calculated the gravitational wave spectrum in an expanding universe, we want to explore the extent to which the phase transition can distinguish between *different expansion histories*. In other words, we would like to interrogate how well a phase transition can serve as a *cosmic witness*. This is important, since growing evidence suggests that the standard assumption of radiation domination prior to Big Bang Nucleosynthesis may be too naive [44, 45]. An early matter dominated era, for example, is motivated by the cosmological moduli problem [46–49], hints from dark matter searches [50–58], and perhaps even baryogenesis [59]. Another possibility of a non-standard expansion history is kination, which we do not cover in this paper but can be explored by our methods [60–66]. We note that gravitational waves have been previously employed to investigate early universe cosmology [67–72].

Our goal is to provide a general theoretical framework to calculate the gravitational wave spectrum in different cosmic expansion histories. This includes scrutiny for changes in different aspects. The dynamics of the phase transition in an expanding universe is studied in Sec. 3, the velocity field power spectrum is calculated in Sec. 4 and the gravitational wave spectrum in Sec. 5. The main findings of the first two aspects are as follows.

---

<sup>1</sup>Note that LISA is also poised to probe hidden sector transitions [22–33] and transitions from multi-step GUT breaking [34–37]

1. The mean bubble separation  $R_*$  is related to  $\beta$  through a generalized relation (Eq. 3.50):

$$R_*(t) = \frac{a(t)}{a(t_f)} (8\pi)^{1/3} \frac{v_w}{\beta(v_w)}, \quad (1.1)$$

where  $t_f$  is the time when the false vacuum fraction is  $1/e$ , at which  $\beta(v_w)$  is evaluated, and  $\beta(v_w)$  can vary by  $\sim 20\%$  for different  $v_w$ . This relation is also confirmed by numerical calculations and is accurate up to an uncertainty of  $2\%$ . If one uses the conformal version of  $R_*$  and  $\beta$ , then they satisfy the same relation as in Minkowski spacetime (see Eq. 3.46).

2. We derived the bubble lifetime distribution in an generic expanding universe in Eq. 3.29, and the conformal lifetime  $\eta_{\text{lt}}$  rather than ordinary lifetime  $t_{\text{lt}}$  should be used. It coincides with the distribution  $e^{-\tilde{T}}$  found in Minkowski spacetime [43] for exponential nucleation.
3. We derived the full set of differential equations in an expanding universe for the fluid and order parameter field model as used in numerical simulations. We find that in the bubble expansion phase the full field equations do not admit rescalings of the quantities that would reduce the expressions to their counterparts in Minkowski spacetime; this rescaling does, however, does work in the bag equation of state model. This implies the velocity profile maintains the same form when appropriate rescalings and variable substitutions are used.
4. We generalized the sound shell model to an expanding universe and calculated the velocity field power spectrum [42, 43].

For the gravitational wave energy density spectrum, the main results are:

1. The peak amplitude of the gravitational wave spectrum visible today has the form (see Eq. 5.45)

$$h^2 \Omega_{\text{GW}} = 8.5 \times 10^{-6} \left( \frac{100}{g_s(T_e)} \right)^{1/3} \Gamma^2 \bar{U}_f^4 \left[ \frac{H_s}{\beta(v_w)} \right] v_w \times \Upsilon. \quad (1.2)$$

Here  $\Gamma \sim 4/3$  is the adiabatic index,  $v_w$  is the wall velocity,  $H_s$  is the Hubble rate when the source becomes active, and  $\Upsilon$  is the suppression factor arising from the finite lifetime,  $\tau_{\text{sh}}$ , of the sound waves. For radiation domination, it is given by

$$\Upsilon = 1 - \frac{1}{\sqrt{1 + 2\tau_{\text{sh}}H_s}}, \quad (1.3)$$

where the standard spectrum generally used corresponds to the asymptotic value  $\Upsilon = 1$  when  $\tau_{\text{sh}}H_s \rightarrow \infty$ . However the onset of non-linear shocks and turbulence which can disrupt the sound wave source occurs at around  $\tau_{\text{sw}}H_s \sim H_s R_*/\bar{U}_f$  where  $\bar{U}_f$  is the root mean square fluid velocity (see Fig. 18). This means the asymptotic value will not be reached and there is a suppression to the standard spectrum. In Fig. 1 we compare our result with the suppression factor recently proposed in [18] (see also [73, 74]). Similarly, the spectrum for matter domination has also been derived in our work and a similar suppression factor  $\Upsilon$  is observed, which has an asymptotic value of  $2/3$ .

2. We find a change to the spectral form, depending upon whether the phase transition occurs during a period of matter or radiation domination. The change in the form is not leading order, due to the fact that the velocity profiles remain largely unchanged and that the autocorrelation time of the source is much smaller than the duration of the transition. This is in contrast to gravitational waves generated from cosmic strings [72]. Even then, the modification of the spectrum

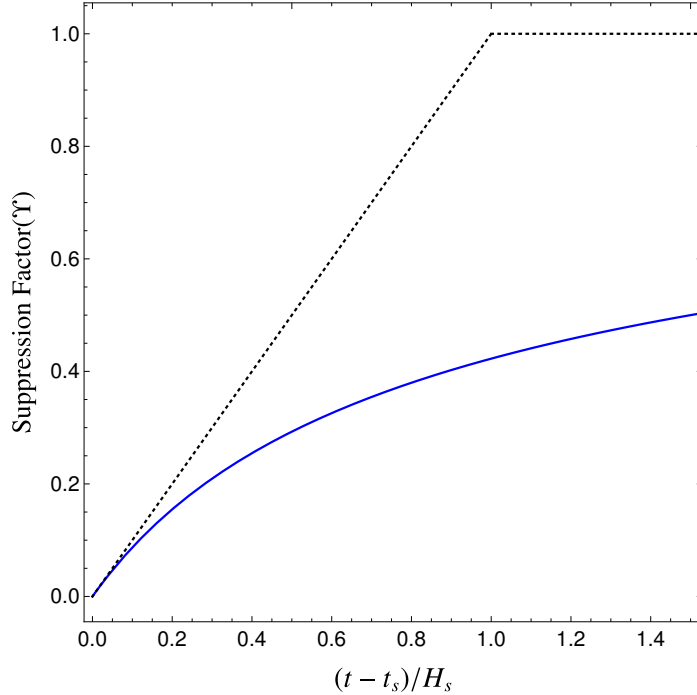


**Figure 1.** The suppression factor (blue solid line) as a function of the elapsed time  $(t - t_s)$  of the source in unit of the Hubble time at  $t_s$  when the source becomes active. The black dashed line denotes  $\text{Min}[\tau_{\text{sh}} H_s, 1]$ .

presents an enticing possibility that the gravitational waves formed during a phase transition can bear witness to an early matter dominated era. We leave a further detailed exploration of the change of the spectral form for future work.

The remainder of this paper is organized as follows. We firstly lay out the theoretical framework for the stochastic gravitational wave calculation in the next Sec. 2 and study the details of the phase transition dynamics in an expanding universe in Sec. 3. After that, we summarize the full set of fluid equations applicable in an expanding universe and study the velocity profile and velocity power spectrum using the sound shell model in Sec. 4. We then analytically calculate the gravitational waves from sound waves in both radiation dominated and matter dominated scenarios in Sec. 5. We summarize our results in Sec. 6.

## 2 Theoretical Framework

In this section, we set up the framework for calculating the stochastic gravitational waves in the presence of a source, which also serves to define our notation. The power spectrum of the gravitational waves, as will be discussed, depends on the unequal time correlator of the source. Therefore this correlator is of central importance in this work and is discussed in the second subsection.

### 2.1 Gravitational Waves

The gravitational wave is the transverse traceless part of the perturbed metric. Neglecting the nonrelevant scalar and vector perturbations, the metric is defined in the FLRW universe as:

$$ds^2 = -dt^2 + a(t)^2(\delta_{ij} + h_{ij}(\mathbf{x}))d\mathbf{x}^2, \quad (2.1)$$

where  $h_{ij}$  is only the transverse traceless part of the perturbed  $3 \times 3$  metric matrix (see, e.g., [75] for a detailed discussion). It is convenient, most often, to work in Fourier space, with the following convention:

$$h_{ij}(t, \mathbf{x}) = \int \frac{d^3q}{(2\pi)^3} e^{i\mathbf{q}\cdot\mathbf{x}} h_{ij}(t, \mathbf{q}), \quad (2.2)$$

where  $\mathbf{q}$  is the comoving wavenumber, in accordance with the comoving coordinate  $\mathbf{x}$ . The physical coordinate is  $a\mathbf{x}$  and the physical wavenumber is  $\mathbf{q}/a$ . The Fourier component  $h_{ij}(t, \mathbf{q})$  is thus of dimension  $-3$ .

Gravitational waves are sourced by the similarly defined transverse traceless part of the perturbed energy momentum tensor of the matter content, defined by

$$\delta T_{ij} = a^2 \pi_{ij}^T + \dots, \quad (2.3)$$

where “ $\dots$ ” denotes the neglected non-relevant parts. Its Fourier transform is defined by

$$\pi_{ij}^T(t, \mathbf{x}) = \int \frac{d^3q}{(2\pi)^3} q e^{i\mathbf{q}\cdot\mathbf{x}} \pi_{ij}^T(t, \mathbf{q}). \quad (2.4)$$

Since  $\pi_{ij}^T$  is of dimension 4, the dimension of its Fourier component  $\pi_{ij}^T(t, \mathbf{q})$  is 1. The Einstein equation leads to a master equation governing the time evolution of each Fourier component of the gravitational waves, which is decoupled from the scalar and vector perturbations,

$$h_{ij}''(t, \mathbf{q}) + 2\frac{a'}{a} h_{ij}'(t, \mathbf{q}) + q^2 h_{ij}(t, \mathbf{q}) = 16\pi G a^2 \pi_{ij}^T(t, \mathbf{q}). \quad (2.5)$$

Here  $\prime \equiv \partial/\partial\eta$ , with  $\eta$  being the conformal time. Derivatives with respect to the coordinate time will be denoted by a dot. The gravitational wave energy density, as denoted by  $\rho_{\text{GW}}$  here, is defined as

$$\rho_{\text{GW}}(t) = \frac{1}{32\pi G} \langle \dot{h}_{ij}(t, \mathbf{x}) \dot{h}_{ij}(t, \mathbf{x}) \rangle, \quad (2.6)$$

with the angle brackets,  $\langle \dots \rangle$ , denoting both the spatial and ensemble average. Due to the overall spatial homogeneity of the universe, we can define the power spectrum of the derivative of the gravitational wave amplitude as:

$$\langle \dot{h}_{ij}(t, \mathbf{q}_1) \dot{h}_{ij}(t, \mathbf{q}_2) \rangle = (2\pi)^3 \delta^3(\mathbf{q}_1 + \mathbf{q}_2) P_h(q_1, t). \quad (2.7)$$

Then the gravitational wave energy density follows

$$\rho_{\text{GW}}(t) = \frac{1}{32\pi G} \frac{1}{2\pi^2} \int dk k^2 P_h(t, q), \quad (2.8)$$

and the gravitational wave energy density spectrum:

$$\frac{d\rho_{\text{GW}}(t)}{d \ln q} = \frac{1}{64\pi^3 G} k^3 P_h(t, q). \quad (2.9)$$

It is conventional to use the dimensionless energy density fraction of the gravitational waves  $\Omega_{\text{GW}}(t) = \rho_{\text{GW}}(t)/\rho_c(t)$  where  $\rho_c$  is the critical energy density at time  $t$ . The corresponding dimensionless version of the spectrum is

$$\mathcal{P}_{\text{GW}}(t, q) \equiv \frac{d\Omega_{\text{GW}}(t)}{d \ln q} = \frac{1}{24\pi^2 H^2} q^3 P_h(t, q) = \frac{1}{24\pi^2 H^2 a^2} q^3 P_{h'}(t, q), \quad (2.10)$$

where in the last step  $P_{h'}(t, q)$  is defined by replacing  $\dot{h}$  with  $h'$  in Eq. 2.7.

We thus need to solve for  $h_{ij}(\eta, \mathbf{q})$  by solving Eq. 2.5 together with equations governing the evolution of the source. We will follow the conventional approach by neglecting the backaction of the metric on the source and calculate the stress tensor with a modelling of the phase transition process. Once  $\pi_{ij}^T(t, \mathbf{q})$  is provided in this way, then  $h_{ij}(t, \mathbf{q})$  can be solved from Eq. 2.5 with Green's function and with the following boundary conditions

$$G(\tilde{\eta} \leq \tilde{\eta}_0) = 0, \quad \frac{\partial G(\tilde{\eta}, \tilde{\eta}_0)}{\partial \tilde{\eta}} \Big|_{\tilde{\eta}=\tilde{\eta}_0^+} = 1, \quad (2.11)$$

where  $\tilde{\eta} = q\eta$ , which is a dimensionless quantity and  $\tilde{\eta}_0$  is the time when the phase transition starts. With the Green's function, the solution of the inhomogeneous Eq. 2.5 is given in terms of the Green's function by

$$h_{ij}(t, \mathbf{q}) = 16\pi G \int_{\tilde{\eta}_0}^{\tilde{\eta}} d\tilde{\eta}' G(\tilde{\eta}, \tilde{\eta}') \frac{a^2(\eta') \pi_{ij}^T(\eta', \mathbf{q})}{q^2}, \quad (2.12)$$

and its derivative with respect to the conformal time follows simply:

$$h'_{ij}(\eta, \mathbf{q}) = 16\pi G \int_{\tilde{\eta}_0}^{\tilde{\eta}} d\tilde{\eta}' \frac{\partial G(\tilde{\eta}, \tilde{\eta}')}{\partial \tilde{\eta}} \frac{a^2(\eta') \pi_{ij}^T(\eta', \mathbf{q})}{q}. \quad (2.13)$$

Then we can calculate the 2-point correlation function:

$$\begin{aligned} \langle h'_{ij}(\eta, \mathbf{q}_1) h'_{ij}(\eta, \mathbf{q}_2) \rangle &= (16\pi G)^2 \int_{\tilde{\eta}_0}^{\tilde{\eta}} d\tilde{\eta}_1 \int_{\tilde{\eta}_0}^{\tilde{\eta}} d\tilde{\eta}_2 \frac{\partial G(\tilde{\eta}, \tilde{\eta}_1)}{\partial \tilde{\eta}} \frac{\partial G(\tilde{\eta}, \tilde{\eta}_2)}{\partial \tilde{\eta}} \\ &\quad \times \frac{a^2(\eta_1) a^2(\eta_2)}{q^2} \langle \pi_{ij}^T(\eta_1, \mathbf{q}_1) \pi_{ij}^T(\eta_2, \mathbf{q}_2) \rangle. \end{aligned} \quad (2.14)$$

Supposing that the gravitational wave generation finishes at  $\tilde{\eta}_f$ , the upper limits for the integrals in the expression above will be  $\tilde{\eta}_f$ . Subsequently, the energy density of the gravitational waves for modes inside the horizon will be simply diluted as  $1/a^4$ . We thus see that at the core of the gravitational wave energy density spectrum calculation is the unequal time correlator (UETC) of  $\pi_{ij}^T$ . It can be parametrized in the following way due to the overall spatial homogeneity of the universe,

$$\langle \pi_{ij}^T(\eta_1, \mathbf{q}_1) \pi_{ij}^T(\eta_2, \mathbf{q}_2) \rangle = \Pi^2(q_1, \eta_1, \eta_2) (2\pi)^3 \delta^3(\mathbf{q}_1 + \mathbf{q}_2). \quad (2.15)$$

It is obvious that the dimension of  $\Pi^2(k, \eta_1, \eta_2)$  is 5.

## 2.2 Unequal Time Correlator of the Fluid Stress Energy Tensor

Let us first write down the energy momentum tensor of the matter content in the universe. Here we keep the dominant contribution from the fluid and assume the fluid velocities are non-relativistic following Ref. [43], then

$$\begin{aligned} T_{ij} &= a^2 [p\delta_{ij} + (p+e)\gamma^2 v^i v^j], \\ T_{i0} &= a [-(p+e)\gamma^2 v^i], \\ T_{00} &= \gamma^2 (e + pv^2), \end{aligned} \quad (2.16)$$

where  $e$  is the energy density,  $p$  is the pressure and the velocity is defined w.r.t the conformal time  $v^i = dx^i/d\eta$ . Then, comparing with Eq. 2.3 and neglecting the non-relevant parts, we have

$$\pi_{ij} = (p+e)\gamma^2 v^i v^j, \quad (2.17)$$

Here the scale factor dependent  $(p + e)$ , takes its homogeneous value (defined with a bar) to leading order  $\bar{e} + \bar{p} \equiv \bar{\omega}$  and scales as  $1/a^4$ .  $\gamma$  is the Lorentz factor. The calculation of the correlator of  $\pi_{ij}^T$  parallels that in Minkowski spacetime:

$$\begin{aligned}
& \langle \pi_{ij}^T(\eta_1, \mathbf{k}) \pi_{ij}^T(\eta_2, \mathbf{q}) \rangle \\
&= \Lambda_{ij,kl}(\hat{\mathbf{k}}) \frac{1}{(2\pi)^6} \int d^3\mathbf{x} \int d^3\mathbf{y} e^{-i\mathbf{k}\cdot\mathbf{x}} e^{-i\mathbf{q}\cdot\mathbf{y}} \langle \pi_{kl}^T(\eta_1, \mathbf{x}) \pi_{ij}^T(\eta_2, \mathbf{y}) \rangle, \\
&= \Lambda_{ij,kl}(\hat{\mathbf{k}}) \bar{\omega}^2 \frac{1}{(2\pi)^6} \int d^3\mathbf{x} \int d^3\mathbf{y} e^{-i\mathbf{k}\cdot\mathbf{x}} e^{-i\mathbf{q}\cdot\mathbf{y}} \langle v^k(\eta_1, \mathbf{x}) v^l(\eta_1, \mathbf{x}) v^i(\eta_2, \mathbf{y}) v^j(\eta_2, \mathbf{y}) \rangle, \\
&= \bar{\omega}^2 \Lambda_{ij,kl}(\hat{\mathbf{k}}) \frac{1}{(2\pi)^{12}} \int d^3\mathbf{q}_1 \int d^3\mathbf{q}_3 \underbrace{\langle \tilde{v}_{\mathbf{q}_1}^k(\eta_1) \tilde{v}_{\mathbf{q}_1-\mathbf{k}}^{l*}(\eta_1) \tilde{v}_{\mathbf{q}_3}^i(\eta_2) \tilde{v}_{\mathbf{q}_3-\mathbf{q}}^{j*}(\eta_2) \rangle}_{\equiv X^{kl ij}}. \tag{2.18}
\end{aligned}$$

Here  $\Lambda_{ij,kl}$  is the standard projection operator and  $\Lambda_{ij,kl}(\hat{k}) = P_{ik}(\hat{k})P_{jl}(\hat{k}) - \frac{1}{2}P_{ij}(\hat{k})P_{kl}(\hat{k})$  with  $P_{ij}(\hat{k}) = \delta_{ij} - \hat{k}^i\hat{k}^j$ .  $\tilde{v}_{\mathbf{q}}^i$  is the Fourier transform of the velocity field  $v^i(\mathbf{x})$ . Due to the nature of the first order phase transition process and according to the central limit theorem,  $\tilde{v}_{\mathbf{q}}^i(\eta)$  follows the Gaussian distribution to a good approximation. Also as in Ref. [43], we neglect the irrotational component, then the two point correlator can be defined in the following way:

$$\langle \tilde{v}_{\mathbf{q}}^i(\eta_1) \tilde{v}_{\mathbf{k}}^{j*}(\eta_2) \rangle = \delta^3(\mathbf{q} - \mathbf{k}) \hat{q}^i \hat{k}^j G(q, \eta_1, \eta_2). \tag{2.19}$$

Any higher order correlator can be reduced to the two point correlator. Defining  $\tilde{\mathbf{q}}_1 \equiv \mathbf{q}_1 - \mathbf{k}$  and  $\tilde{\mathbf{q}}_3 \equiv \mathbf{q}_3 - \mathbf{q}$ , then

$$\begin{aligned}
X^{kl ij} &= \langle \tilde{v}_{\mathbf{q}_1}^k(\eta_1) \tilde{v}_{\mathbf{q}_1}^{l*}(\eta_1) \rangle \langle \tilde{v}_{\mathbf{q}_3}^i(\eta_2) \tilde{v}_{\mathbf{q}_3}^{j*}(\eta_2) \rangle + \langle \tilde{v}_{\mathbf{q}_1}^k(\eta_1) \tilde{v}_{\mathbf{q}_3}^i(\eta_2) \rangle \langle \tilde{v}_{\mathbf{q}_1}^{l*}(\eta_1) \tilde{v}_{\mathbf{q}_3}^{j*}(\eta_2) \rangle \\
&\quad + \langle \tilde{v}_{\mathbf{q}_1}^k(\eta_1) \tilde{v}_{\mathbf{q}_3}^{j*}(\eta_2) \rangle \langle \tilde{v}_{\mathbf{q}_1}^{l*}(\eta_1) \tilde{v}_{\mathbf{q}_3}^i(\eta_2) \rangle. \tag{2.20}
\end{aligned}$$

The first term contributes trivially to  $\mathbf{k} = 0$  and, collecting all other contributions, we have

$$\langle \pi_{ij}^T(\eta_1, \mathbf{k}) \pi_{ij}^T(\eta_2, \mathbf{q}) \rangle = \delta^3(\mathbf{k} + \mathbf{q}) \bar{\omega}^2 \frac{1}{(2\pi)^6} \int d^3\mathbf{q}_1 G(q_1, \eta_1, \eta_2) G(\tilde{q}_1, \eta_1, \eta_2) (1 - \mu^2)^2 \frac{q_1^2}{\tilde{q}_1^2}. \tag{2.21}$$

Comparing with Eq. 2.15, it follows that

$$\Pi^2(k, \eta_1 - \eta_2) = \bar{\omega}^2 \int \frac{d^3q}{(2\pi)^3} G(q, \eta_1, \eta_2) G(\tilde{q}, \eta_1, \eta_2) \frac{q^2}{\tilde{q}^2} (1 - \mu^2)^2, \tag{2.22}$$

where  $\tilde{q} = |\mathbf{q} - \mathbf{k}|$  and  $\mu = \hat{\mathbf{q}} \cdot \hat{\mathbf{k}}$ . Here  $\Pi^2$  depends on  $\eta_1 - \eta_2$  rather than on  $\eta_1$  and  $\eta_2$  separately. This is because the source is largely stationary.

We will later see that the fluid equations maintain the same form as in the Minkowski spacetime once properly rescaled quantities and previously defined  $v^i(\mathbf{x})$  are used (see also Ref. [39]). In particular it means that we can define a rescaled stress energy tensor ( $\tilde{\pi}_{ij}^T$ ) for the fluid:

$$\pi_{ij}^T(\mathbf{q}, \eta) = \frac{a_s^4}{a^4(\eta)} \tilde{\pi}_{ij}^T(\mathbf{q}, \eta), \tag{2.23}$$



where  $a_s$  is a reference scale factor when the source becomes active. Similarly we can define a rescaled and dimensionless two point correlator  $\tilde{\Pi}$  by

$$\Pi^2(q, t_1, t_2) \equiv \frac{a_s^8}{a^4(\eta_1)a^4(\eta_2)} [(\bar{\epsilon} + \bar{p}) \bar{U}_f^2]^2 L_f^3 \tilde{\Pi}^2(qL_f, q\eta_1, k\eta_2), \quad (2.24)$$

where  $\bar{\epsilon}$  and  $\bar{p}$  are the rescaled average energy density and pressure, which correspond to the quantities measured at  $t_s$ . The quantity  $\bar{U}_f$  describes the magnitude of the fluid velocity and is dimensionless. The correlator,  $\Pi^2$ , on the left hand side of the equation has dimension 5. Therefore, the additional length factor  $L_f^3$  is inserted here to make  $\tilde{\Pi}$  dimensionless. Since this length scale is free from the effect of the expanding universe, it is a comoving length scale. It is found from numerical simulations [39, 40] that the typical scale in the gravitational wave production is the (comoving) mean bubble separation  $R_{*c}$ . So we will choose  $L_f = R_{*c}$ .

The calculation of the UETC requires us to scrutinize the entire process of the phase transition and the gravitational wave production. This task can be separated into two parts. The first part is a study of the bulk parameters characterizing the process of the phase transition, which we will perform in the next section. The second part is understanding the evolution of the source, which we go on to perform in Sec. 4.

### 3 Dynamics of the Phase Transition

In this section, we study the changes to the dynamics of the phase transition in an expanding universe. This includes parameters characterizing the behavior of the bubble formation, expansion and percolation: the bubble nucleation rate, the fraction of the false vacuum and the unbroken area of the walls at a certain time. These will eventually be incorporated in the calculation of the velocity power spectrum in the sound shell model. Another set of important quantities characterize the statistics of the bubbles ever formed: the bubble lifetime distribution, as well as the bubble number density. These are also needed in the velocity power spectrum calculation. Moreover, the timing of some important steps in the phase transition are also included, like the nucleation temperature and the percolation temperature. Other changes to the parameters entering the gravitational wave power spectrum calculation are also included, with  $\beta/H$  a representative example. We now proceed to a detailed discussion of these quantities.

#### 3.1 Bubble Nucleation Rate

The first and most basic ingredient in the analysis of a first order cosmological phase transition is the nucleation rate of the bubbles in the meta-stable vacuum at finite temperature [76, 77]. The number of bubbles nucleated per time per physical volume is given by the following formula:

$$p = p_0 \exp \left[ -\frac{S_{3,b}(T)}{T} \right]. \quad (3.1)$$

Here  $S_3$  is the Euclidean action of the underlying scalar field  $\vec{\phi}$  that minimizes the solution

$$S_3(\vec{\phi}, T) = 4\pi \int dr r^2 \left[ \frac{1}{2} \left( \frac{d\vec{\phi}(r)}{dr} \right)^2 + V(\vec{\phi}, T) \right], \quad (3.2)$$

with the following bounce boundary conditions:

$$\left. \frac{d\vec{\phi}(r)}{dr} \right|_{r=0} = 0, \quad \vec{\phi}(r = \infty) = \vec{\phi}_{\text{out}}, \quad (3.3)$$

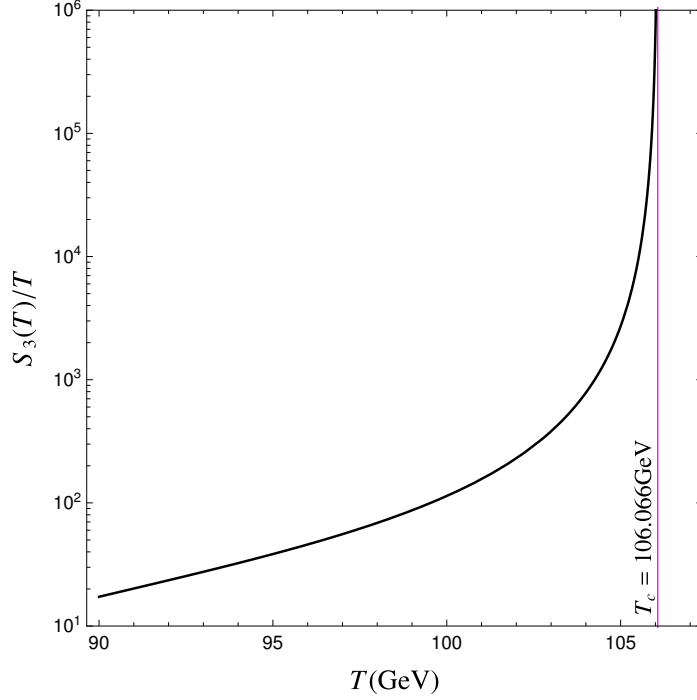


**Figure 2.** The representative profile of  $S_3(T)/T$  for the example used in Sec. 3. See Appendix. A for more details on how to reproduce this.

where  $\vec{\phi}_{\text{out}}$  are the components of the vev outside the bubble. For the pre-factor, we see that  $p_0 \propto T^4$  on dimensional grounds, while its precise determination requires integrating out fluctuations around the bounce solution (see e.g., [78, 79] for detailed calculations or [80] for a pedagogical introduction).

The function  $S_3(T)/T$  generally starts from infinity at  $T_c$  and drops sharply as temperature decreases, with a typical profile shown in Fig. 20. Bubbles will be nucleated within a short range of time, say at  $t_*$ , when this rate changes slowly, which admits the following Taylor expansion:

$$p(t) = p_0 \exp[-S_* + \beta(t - t_*)], \quad (3.4)$$

where  $S_* \equiv S_3(T_*)/T_*$ ,  $\beta \equiv d \ln p(t)/dt|_{t=t_*}$ <sup>2</sup>. More explicitly, we have

$$\frac{S_3}{T} = \frac{S_3}{T} \Big|_{t_*} + \underbrace{\frac{d(S_3/T)}{dT} \frac{dT}{dt} \Big|_{t=t_*}}_{\equiv -\beta} (t - t_*), \quad (3.6)$$

and thus

$$\frac{\beta}{H_*} = -\frac{1}{H_*} \frac{dT}{dt} \frac{d(S_3/T)}{dT} \Big|_{t=t_*}. \quad (3.7)$$

<sup>2</sup> If there exists a barrier at zero temperature, then  $S_3(T)/T$  will reach a minimum, say at  $t_*$ . The rate can be expanded around the minimum:

$$p(t) = p_0 \exp \left[ -S_* - \frac{1}{2} \beta_2^2 (t - t_*)^2 \right], \quad (3.5)$$

with  $\beta_2 \equiv S'''(t_*)$  and the first derivative vanishing. The bubble nucleation will happen mostly around  $t_*$ , making it look like an instantaneous nucleation [42].

We will later see how  $t_*$  should be chosen. For now, we provide a generic expression for  $\beta$  during an expanding universe, which needs the relation between  $t$  and  $T$ . Suppose the universe is expanding as  $a = c_a t^n$  and the radiation sector is expanding adiabatically such that entropy is conserved per comoving volume:

$$s_R(T)a^3 = \text{const.} \quad (3.8)$$

Here  $s_R \propto T^3$ , giving then  $T \propto 1/a \propto t^{-n}$ . This is the case for a radiation dominated universe, and for a matter dominated universe where the non-relativistic matter does not inject entropy to the radiation sector. However when the matter decays into radiation, entropy injection into the radiation sector gives a different dependence  $T \propto a^{-3/8}$  [81]. Generically, we can assume

$$T \propto a^{-\gamma}, \quad (3.9)$$

which then leads to  $T = c_T t^{-n\gamma}$ , with  $c_T$  being another constant. We thus have

$$\frac{dT}{dt} = -c_T n\gamma t^{-n\gamma-1}. \quad (3.10)$$

Moreover  $H = \dot{a}/a = n/t$ . Then

$$\frac{1}{H} \frac{dT}{dt} = -c_T \gamma t^{-n\gamma} = -\gamma T. \quad (3.11)$$

Therefore  $\beta/H_*$  reduces to the following form

$$\frac{\beta}{H_*} = \gamma T \left. \frac{d(S_3/T)}{dT} \right|_{t=t_*}. \quad (3.12)$$

It is obvious from this result that  $\beta/H_*$  does not depend on  $n$ , i.e., it does not depend on how the scale factor evolves with time but rather on how  $T$  decreases with the scale factor through  $\gamma$ . For both the standard radiation dominated universe and an early matter dominated universe wherein the matter is decoupled from the radiation,  $\gamma = 1$ . For the matter dominated universe wherein the matter decays into radiation,  $\gamma = 3/8$ , which gives a smaller  $\beta/H_*$ .

### 3.2 False Vacuum Fraction

The false vacuum fraction  $g(t_c, t)$  at  $t > t_c$  can be obtained following the derivation in Ref. [82]

$$g(t_c, t) = \exp \left[ -\frac{4\pi}{3} \int_{t_c}^t dt' p(t') a^3(t') r(t', t)^3 \right] \equiv \exp[-I(t)]. \quad (3.13)$$

Here  $I(t)$  corresponds to the volume of nucleated bubbles per comoving volume, double counting the overlapped space between bubbles and virtual bubbles within others.  $r(t', t)$  is the comoving radius of the bubble nucleated at  $t'$  and measured at  $t$ ,

$$r(t', t) = \int_{t'}^t dt'' \frac{v_w}{a(t'')}. \quad (3.14)$$

For Minkowski spacetime,  $r(t', t) = v_w(t - t')$ . For a FLRW spacetime  $r(t', t) = v_w(\eta' - \eta)$ , which takes the same form as the Minkowski spacetime, irrespective of the detailed expansion behavior, when conformal time is used. In obtaining the above results, a constant bubble wall velocity  $v_w$  has

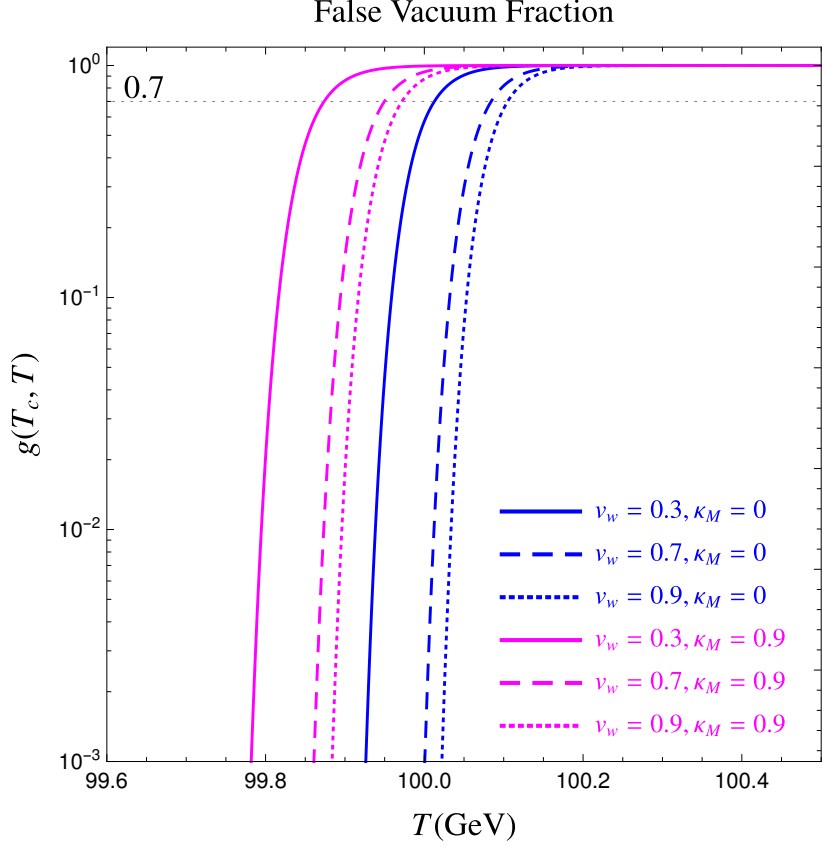


**Figure 3.** The false vacuum fraction as defined Eq. 3.13 for different fractions of matter energy density at  $T_c$  ( $\kappa_M = 0, 0.9$ , defined in Eq. 3.18) and for several bubble wall velocities ( $v_w = 0.3, 0.7, 0.9$ ). The case of  $\kappa_M = 0$  corresponds to a radiation dominated universe and  $\kappa_M = 0.9$  for matter domination. The horizontal line at  $g = 0.7$  is roughly the time when the bubbles percolate.

been assumed and the initial size of the bubble has been neglected. This is justified as the initial size is very small.

Eq. 3.13 can be recast in a form that is convenient for calculations, in terms of the temperature. Suppose that the scale factor at the time of the critical temperature is  $a_c$  and that the scale factor at a later time is related to it by

$$\frac{a}{a_c} \equiv \left( \frac{T_c}{T} \right)^{1/\gamma}. \quad (3.15)$$

The comoving bubble radius can be conveniently expressed with an integral over temperature:

$$r(T', T) = \frac{v_w}{a_c} \int_T^{T'} \frac{dT''}{T''} \frac{1}{\gamma H(T'')} \left( \frac{T_c}{T''} \right)^{-1/\gamma}. \quad (3.16)$$

Accordingly  $I(T)$  can be written as

$$I(T) = \frac{4\pi}{3} \int_T^{T_c} \frac{dT'}{T'} \frac{1}{\gamma H(T')} \bar{p}_0 T'^4 \exp \left[ -\frac{S_3(T')}{T'} \right] \left( \frac{T_c}{T'} \right)^{3/\gamma} [a_c r(T', T)]^3. \quad (3.17)$$

Here the  $\bar{p}_0$  is defined by  $p_0 = \bar{p}_0 T^4$  and we choose  $\bar{p}_0 = 1$  in the examples of analysis as is usually done in the literature. A different choice of  $\bar{p}_0$  would, of course, affect the resulting false vacuum fraction and thus the relevant temperatures defined [83]. Since the focus here is on the changes due to different expansion histories, a fixed choice of  $\bar{p}_0$  serves our purpose well. For the Hubble rate, we need to be more precise with regard to the matter content. We consider a universe consisting of both radiation and non-relativistic matter and define  $\kappa_M$  to be the fraction of the total energy density at  $T_c$  that is non-relativistic matter:

$$\kappa_M = \left. \frac{\rho_{\text{Matter}}}{\rho_{\text{Total}}} \right|_{T=T_c}. \quad (3.18)$$

We also neglect the vacuum energy for these examples, though it certainly exists during a phase transition.

$$H = H(T_c) \sqrt{\frac{\kappa_M}{y^3} + \frac{1 - \kappa_M}{y^4}}, \quad (3.19)$$

where  $y = a/a(T_c)$ . We show in Fig. 3 the false vacuum fraction during the phase transition, for a purely radiation dominated universe with  $\kappa_M = 0$  and a matter dominated one with  $\kappa_M = 0.9$ , and for three choices of bubble wall velocities  $v_w = 0.3, 0.7, 0.9$ . For both choices of  $\kappa_M$ , it is clear from these figures that increasing  $v_w$  speeds up the process of phase transition. From  $\kappa_M = 0$  to  $\kappa_M = 0.9$ , a larger energy density and thus a larger Hubble rate is obtained, which decreases the function  $r(T', T)$  and  $I(I)$  and thus slows down the drop of  $g(T_c, T)$ .

One often encounters the percolation temperature, which is defined such that the fraction in true vacuum is about 30% of the total volume [73], i.e., when

$$g(T_c, T_p) \approx 0.7, \quad \text{or} \quad I(T_p) \approx 0.34, \quad (3.20)$$

and corresponds intersection points of the horizontal line with the curves in Fig. 3.

### 3.3 Unbroken Bubble Wall Area

With the false vacuum fraction in Eq. 3.13, the unbroken bubble wall area during the phase transition can be derived [43] and will be used in the derivation of the bubble lifetime distribution. Consider a comoving volume of size  $V_c$  and a sub-volume occupied by false vacuum  $V_{c,\text{False}}$ . Then the comoving unbroken bubble wall area  $\mathcal{A}_c(t)$  at  $t$  satisfies the following relation:

$$dg(t_0, t) = \frac{dV_{c,\text{False}}}{V_c} = -\mathcal{A}_c(t) \frac{v_w dt}{a(t)} = -\mathcal{A}_c(t) v_w d\eta. \quad (3.21)$$

Then  $\mathcal{A}_c$  is given by

$$\mathcal{A}_c(t) = -\frac{1}{v_w} \frac{dg(t_0, t)}{d\eta} = a(\eta) \frac{H(T) \gamma T}{v_w} \frac{dg(T_c, T)}{dT}. \quad (3.22)$$

One can also define the proper area per proper volume

$$\mathcal{A} = \frac{\text{Proper Area}}{\text{Proper Volume}} = \frac{a^2 \times \text{Comoving Area}}{a^3 \times \text{Comoving Volume}} = \frac{1}{a} \mathcal{A}_c. \quad (3.23)$$

Since  $\mathcal{A}_c(t)$  and  $\mathcal{A}$  are the area per volume, they are of dimension 1, and can be presented in units of  $m^{-1}$  or GeV. A more meaningful representation can be obtained by comparing it with the typical

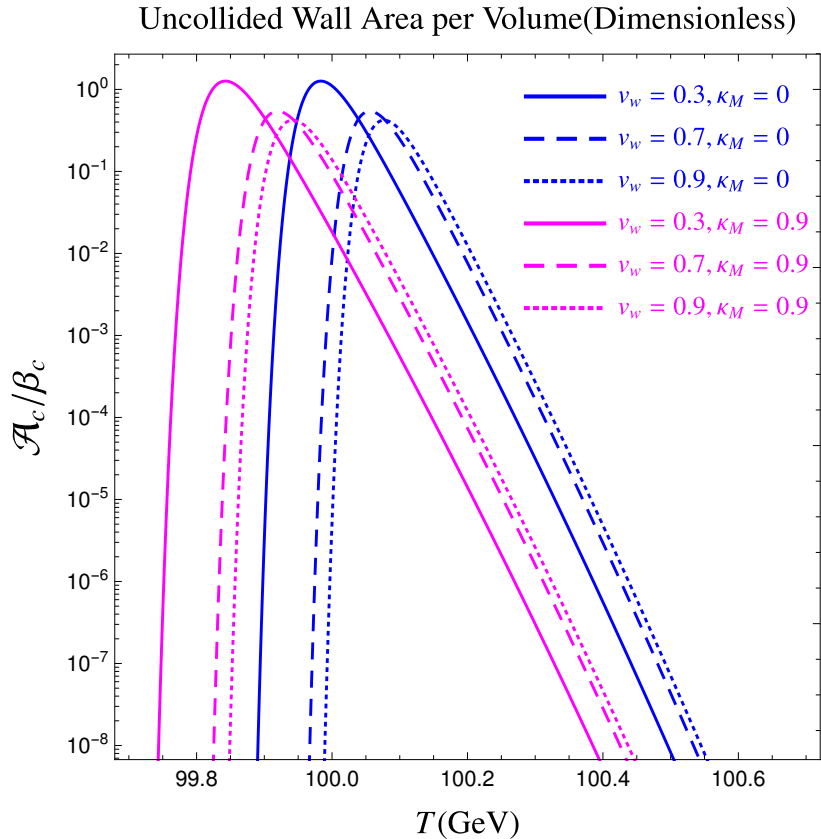


**Figure 4.** The dimensionless comoving uncollided bubble wall area as defined in Eq. 3.22 and Eq. 3.41 for different values of  $\kappa_M$  (defined in Eq. 3.18) and  $v_w$ .

scale at the corresponding temperature. One such quantity is  $\beta_c$ , to be defined later, which is the comoving version of the  $\beta$  parameter and is related to the mean bubble separation (also to be defined later). We show  $\mathcal{A}_c/\beta_c$  in Fig. 4 for different choices  $\kappa_M$  and  $v_w$ , similar to what are used in Fig. 3. We can see the area first increases as more bubbles are formed and expanding. It decreases as bubbles collide with each other and the remaining false vacuum volume is shrinking to zero. The different behaviors when changing  $v_w$  and the amount of non-relativistic matter contents coincide with what we observe in Fig. 3.

### 3.4 Bubble Lifetime Distribution

The bubble lifetime distribution describes the distribution of bubble lifetime for all the bubbles ever formed and destroyed during the entire process of the phase transition. This can be obtained with the help of the unbroken bubble wall area derived earlier, by generalizing the result derived in Ref. [43] to the expanding universe. We start by considering the number of bubbles that are created at  $t'$  and are destroyed with comoving radius  $r$ . Here a bubble is defined as destroyed when approximately half of its volume is occupied by the expanding true vacuum space. These bubbles are therefore at a comoving distance of  $r$  at  $t'$  from the part of the unbroken bubble wall, assuming constant and universal bubble wall velocity  $v_w$ . The time  $t$  when this set of bubbles is destroyed is connected with

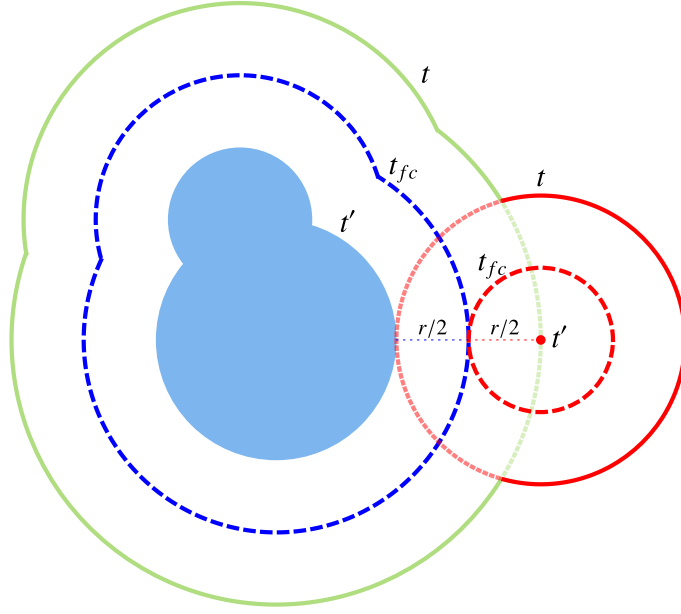


**Figure 5.** Illustration for the calculation of the bubble lifetime distribution. At  $t'$ , there is a central blue blob composed of two already collided bubbles depicting a region of true vacuum space which is expanding into the surrounding false vacuum space, and also a small red nucleus denoting a bubble starting to form. At this time, the comoving distance between the red dot and the nearest blue boundary is  $r$ . At  $t_{fc}$ , the walls of the blue blob and the fledged red bubble advance to the place denoted by blue and red dashed circles respectively, where they make the first contact. At  $t$ , they reach the place denoted by the solid blue and red circles, where half of the red bubble is devoured by the blue one, and the red bubble is defined to be destroyed with a final radius  $r$ .

$t'$  and  $r$  by

$$r = \int_{t'}^t \frac{v_w dt''}{a(t'')}. \quad (3.24)$$

Since only two quantities out of  $(r, t', t)$  are independent, we denote  $\mathcal{A}_c(t(t', r))$  as  $\mathcal{A}_c(t', r)$  and define the number of bubbles per comoving volume as  $n_{b,c}$ . We then have (see an illustration and more details in Fig. 5):

$$d^2 n_{b,c} = p(t') [a^3(t') \mathcal{A}_c(t', r) dr] dt'. \quad (3.25)$$

This implies that:

$$d \left( \frac{dn_{b,c}}{dr} \right) \equiv dn_{b,c}(r) = p(t') [a^3(t') \mathcal{A}_c(t', r)] dt'. \quad (3.26)$$

Now, for fixed  $r$ , we consider all the bubbles ever formed before a time  $t_f$ :

$$n_{b,c}(r)|_{t_c}^{t_f} = \int_{t_c}^{t_f} dt' p(t') [a^3(t') \mathcal{A}_c(t', r)], \quad (3.27)$$

and  $n_{b,c}(r) = 0$  at  $t_c$  for all  $r$ . Consider a time when all bubbles have disappeared, when  $t_f$  is large enough. Now  $n_{b,c}(r)|_{t_f}$  becomes a constant  $\tilde{n}_{b,c}(r)$ . We can then relate  $r$  with the lifetime of the

bubbles. For the bubble nucleated at  $t'$  and destroyed at  $t$ , we have

$$r = \int_{t'}^t dt'' \frac{v_w dt''}{a(t'')} = v_w \eta_{lt}, \quad (3.28)$$

where  $\eta_{lt}$  is the conformal lifetime of the bubble. Thus,  $r$  has the same relation with the conformal lifetime as its relation with  $t_{lt}$  in Minkowski spacetime. We can therefore proceed to derive a conformal lifetime distribution for all bubbles ever formed and destroyed:

$$\tilde{n}_{b,c}(\eta_{lt}) \equiv \frac{dn_{b,c}}{d\eta_{lt}} = v_w \tilde{n}_{b,c}(r) = v_w \int_{t_c}^{t_f} dt' p(t') a^3(t') \mathcal{A}_c(t', v_w \eta_{lt}). \quad (3.29)$$

Remember  $\mathcal{A}_c(t', v_w \eta_{lt}) = \mathcal{A}_c(t(t'), v_w \eta_{lt})$  and it is evaluated at  $t$ , which should be determined through Eq. 3.28 given  $t'$  and  $\eta_{lt}$ . To present a numerically convenient representation of the above result, we convert coordinate time  $t$  to conformal time  $\eta$  and then to temperature. For the bubble formed at  $t'$ , the corresponding conformal time is related to temperature by

$$\eta' - \eta_c = \int_{t_c}^{t'} \frac{dt''}{a(t'')} = \frac{1}{a_c} \int_{T'}^{T_c} \frac{dT''}{T''} \frac{1}{\gamma H(T'')} \left( \frac{T_c}{T''} \right)^{-1/\gamma} \equiv \Delta\eta(T', T_c). \quad (3.30)$$

Then for the bubble with conformal lifetime  $\eta_{lt}$ , the conformal time for its destruction is given by  $\eta_{lt} + (\eta' - \eta_c)$ , with the corresponding temperature  $T$  determined through

$$\eta_{lt} + (\eta' - \eta_c) = \Delta\eta(T, T_c). \quad (3.31)$$

This temperature, or time, is what should be used in  $\mathcal{A}_c$ , rather than  $T'$ . With the relation between  $T$  and  $T'$  found, it is then straightforward to do the integral in Eq. 3.29, which requires only converting  $t'$  to temperature.

### 3.5 Bubble Number Density

The evolution of the number density per proper volume  $n_b = N_b/V$  is governed by the following equation

$$\frac{d[n_b a^3(t)]}{dt} = p(t) g(t_c, t) a^3(t), \quad (3.32)$$

which can be integrated to give (noting that  $n_b(t_c) = 0$ ):

$$n_b(t) = \frac{1}{a^3(t)} \int_{t_c}^t dt' p(t') g(t_c, t') a^3(t'). \quad (3.33)$$

This does not include the decrease of bubble number due to collisions and  $n_b$  thus includes all the bubbles ever formed. The result for  $n_b(t)$  can be similarly transformed into a function of temperature.

$$n_b(T) = \left( \frac{T}{T_c} \right)^{3/\gamma} \int_T^{T_c} \frac{dT'}{T'} \frac{1}{\gamma H(T')} \bar{p}_0 T'^4 \exp \left[ -\frac{S_3(T')}{T'} \right] g(T_c, T') \left( \frac{T_c}{T'} \right)^{3/\gamma}. \quad (3.34)$$

We show  $n_b$  in units of  $m^{-3}$  in the left panel of Fig. 6 and the total bubble number per Hubble volume  $n_b/H^3(T)$  in the right panel. We can see that the bubble number density increases for a delayed false



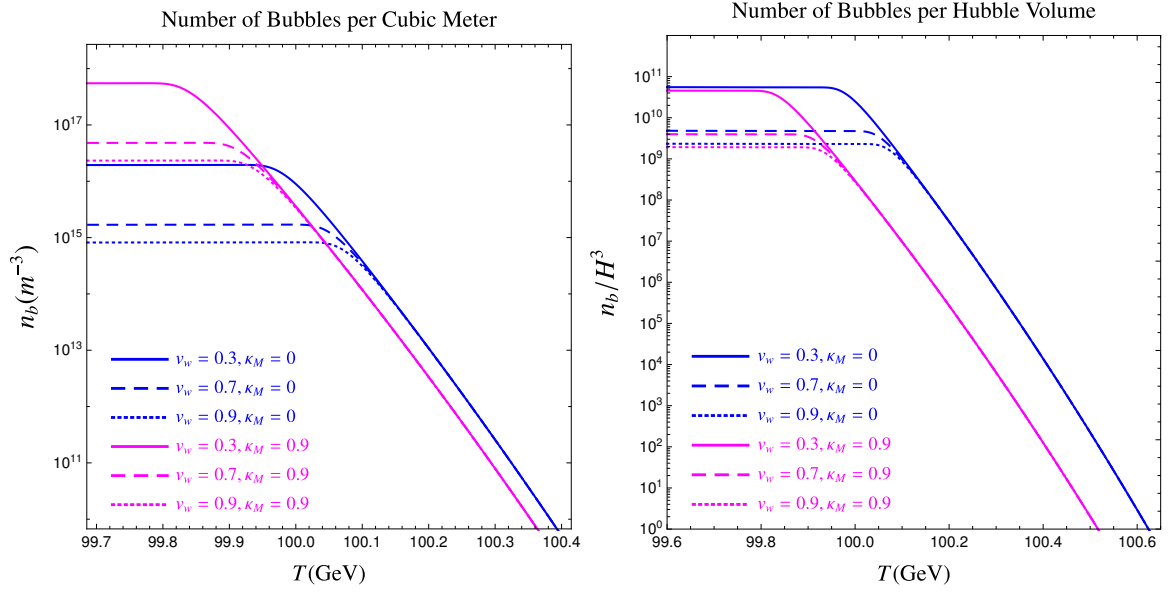


**Figure 6.** The number of bubbles (see Eq. 3.33) per  $m^3$ (left) and per Hubble volume(right) as a function of temperature for difference fractions of non-relativistic matter content at the critical temperature  $\kappa_M$  (defined in Eq. 3.18) and for different bubble wall velocities  $v_w$ .

vacuum fraction, which is consistent with physical intuition. From  $n_b$ , we can define the mean bubble separation,  $R_*$ , as

$$R_*(t) = \left[ \frac{V(t)}{N_b(t)} \right]^{1/3} = \left[ \frac{1}{n_b(t)} \right]^{1/3}. \quad (3.35)$$

This is shown in Fig. 7. For both  $n_b$  and  $R_*$ , it appears they both reach an asymptotic value after the bubbles have disappeared when the curves in these figures become flat. This is misleading as after the time the bubbles have disappeared,  $n_b$  will be diluted as  $1/a^3$  and accordingly  $R_*$  increases as  $a$ . The flat curves in the figures are simply due to the very tiny change of temperature plotted. From numerical simulations [39, 40], it is found that the peak frequency of the gravitational wave spectrum is related to  $R_*$ . Therefore any change on  $R_*$  will translate into a shift of the peak frequency of the gravitational waves. Since  $R_*$  is of particular importance, it is convenient to use the comoving version of it  $R_{*c} = (V_c/N_b)^{1/3}$ , which will reach an asymptotic value after the bubble disappearance.

From the right panel of Fig. 6, we can easily read off the nucleation temperature  $T_n$ , which is defined such that at this temperature there is about one bubble within a Hubble volume [84]. Note  $T_n$  obtained this way differs slightly from the usually used, and a bit crude, criterion:

$$\int_{t_c}^{t_n} dt \frac{p(t)}{H(t)^3} = 1, \quad (3.36)$$

which for radiation dominated universe where  $H^2 = 8\pi G\rho/3$  and  $\rho = \frac{\pi^2}{30}g_*(T)T^4$  translates into the condition:

$$\int_{T_n}^{T_c} \frac{dT}{T} \left( \frac{90}{8\pi^3 g_*} \right)^2 \left( \frac{m_{\text{Pl}}}{T} \right)^4 \exp \left[ -\frac{S_3(T)}{T} \right] = 1. \quad (3.37)$$

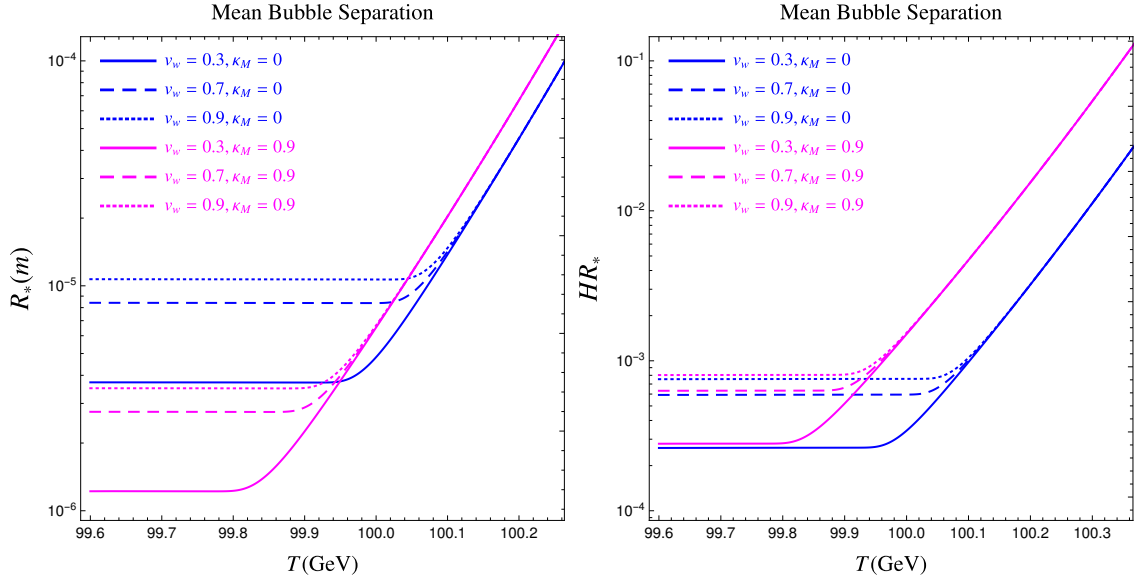


**Figure 7.** Mean bubble separation  $R_*$  (defined in Eq. 3.35) for different fractions of the non-relativistic matter content at the critical temperature  $\kappa_M$  and for different bubble wall velocities  $v_w$ . The left panel is in unit of meter and the right in unit of Hubble radius.

Here  $m_{\text{pl}}$  is the Planck mass. A further simplification says that  $T_n$  is determined by  $S_3(T_n)/T_n = 140$  [84]. These determined  $T_n$  differs slightly from the more accurate result obtained by solving directly for  $n_b$  with Eq. 3.32.

### 3.6 Relation between $\beta$ and Mean Bubble Separation ( $R_*$ )

It was found from numerical simulations that the peak of the gravitational wave power spectrum is located at  $kR_* \sim 10$  [40], where  $R_*$  is the mean bubble separation defined earlier. However the standard spectrum people generally use is expressed in terms of  $\beta$  (see, e.g., [1, 2]). So the relation between  $\beta$  and  $R_*$  is needed. It can be derived analytically under reasonable assumptions as was shown in Ref. [43], which says

$$R_* = \frac{(8\pi)^{1/3}}{\beta(v_w)} v_w. \quad (3.38)$$

Here we emphasize that  $\beta$  varies when  $v_w$  is changed. The question is then will this relation still hold in an expanding universe. We give a detailed derivation here, which parallels and generalizes the derivation in Ref. [43].

We rewrite Eq. 3.32 in terms of the conformal time (we still use the same function labels though  $t$  is replaced by  $\eta$ )

$$\frac{d(n_{b,c})}{d\eta} = p(\eta)g(\eta_c, \eta)a^4(\eta), \quad (3.39)$$

where  $n_{b,c} = n_b a^3$  and is the comoving bubble number density. Here the false vacuum fraction  $g$  decreases sharply when its exponent  $I(T)$  becomes of order 1. Since  $p(\eta)$  increases exponentially, there is a peak for the r.h.s in above equation, at which time the bubbles are mostly nucleated. As  $g$  decreases much more sharply than  $p$  increases, the rate  $p$  only increases slowly during this time

duration and it can be Taylor expanded at around this time. This time can be conveniently chosen to be  $\eta_0$  which satisfies  $I(\eta_0) = 1$ . Then similarly to Eq. 3.4, we define a Taylor expansion but w.r.t the conformal time:

$$p(\eta) = p_0(\eta_0)\exp[-S_0 + \beta_c(\eta - \eta_0)], \quad (3.40)$$

where we have neglected the very slow change of  $p_0(\eta)$  and defined a comoving version of  $\eta$ :

$$\beta_c = \left. \frac{d \ln p}{d\eta} \right|_{\eta=\eta_0}. \quad (3.41)$$

Now lets see how  $n_{b,c}$  in Eq. 3.39 can be solved in terms of  $\beta_c$ . To do it, lets firstly see how  $g$  or its exponent  $I$  can be expressed in terms of  $\beta_c$ . From Eq. 3.13, we can write  $I$  in the following way:

$$\begin{aligned} I(\eta) &= \frac{4\pi}{3} \int_{\eta_c}^{\eta} d\eta' a^4(\eta') p(\eta') r(\eta', \eta)^3 \\ &= \frac{4\pi}{3} v_w^3 \int_{\eta_c}^{\eta} d\eta' p_0(\eta_0) e^{-S_0 + \beta_c(\eta' - \eta_0)} (\eta - \eta')^3 \\ &= 8\pi \frac{v_w^3}{\beta_c^4} p_0(\eta_0) e^{-S_0 + \beta_c(\eta - \eta_0)}. \end{aligned} \quad (3.42)$$

Now define a time  $\eta_f$  such that

$$I(\eta_f) = 1, \quad (3.43)$$

then at a later time much simpler expressions can be obtained:

$$I(\eta) = e^{\beta_c(\eta - \eta_f)}, \quad g(\eta_c, \eta) = e^{-I(\eta)}. \quad (3.44)$$

As  $I(\eta)$  depends on the bubble wall velocity  $v_w$ , the resulting  $t_f$  and more importantly  $\beta_c$  is a function of  $v_w$ . Plug above expressions of  $g(\eta_c, \eta)$ ,  $p(\eta)$  into Eq. 3.39, and integrate over  $\eta$ , we have

$$n_{b,c} = \frac{1}{\beta_c} p_0(\eta_0) e^{-S_0 + \beta_c(\eta_f - \eta_0)} = \frac{\beta_c^3(v_w)}{8\pi v_w^3}. \quad (3.45)$$

Here the second equality comes from the relation in Eq. 3.43. As noted in Ref. [43], the best choice of  $t_0$  is  $t_f$  so that the Taylor expansion of  $p(\eta)$  converges more quickly. This result gives the relation between the comoving mean bubble separation  $R_{*c}$  and  $\eta_c$ :

$$R_{*c} = (8\pi)^{1/3} \frac{v_w}{\beta_c(v_w)}. \quad (3.46)$$

We can also write all results in terms of physical quantities. From Eq. 3.41 and enforcing  $t_0 = t_f$ , we have

$$\beta_c = a(\eta_f)\beta = a(\eta_f) \left[ \gamma H(T) T \frac{d(S_3/T)}{dT} \right] \Big|_{T=T_f}, \quad (3.47)$$

and thus

$$n_{b,c} = a^3(\eta_f) \frac{\beta^3}{8\pi v_w^3}. \quad (3.48)$$

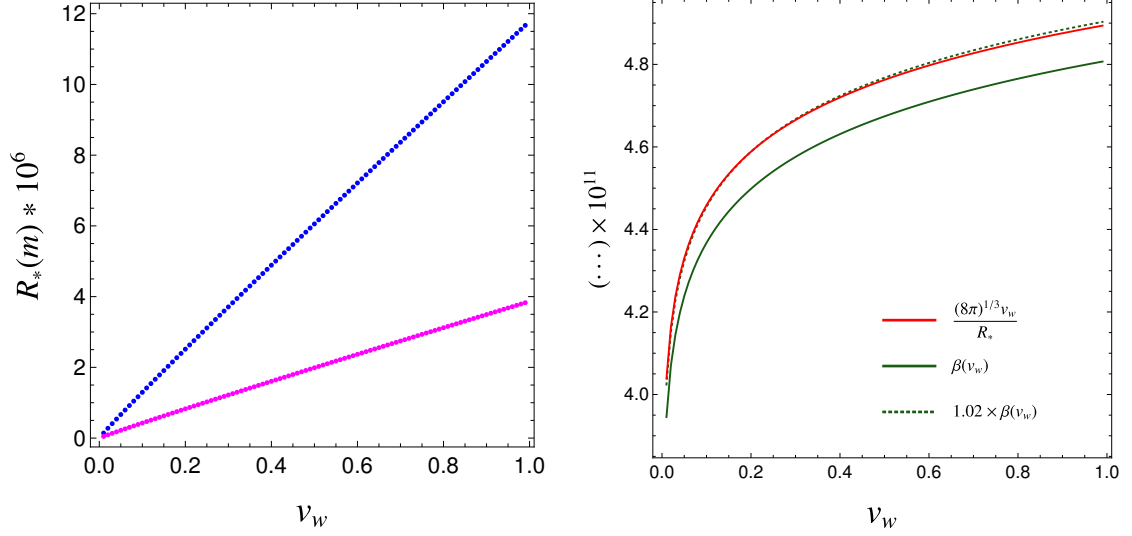


**Figure 8.** The left panel shows the mean bubble separation  $R_*$  immediately after all the bubbles have disappeared versus bubble wall velocity  $v_w$ . The right panel shows  $\beta(v_w)$  calculated using Eq. 3.7 at  $t_f$ , as compared with that calculated using  $R_*$  using Eq. 3.50. The dotted line shows these differ by roughly 2%.

Note  $n_{b,c}$  becomes a constant number as  $N_b$  reaches its maximum and the comoving volume is fixed. The physical number density after all the bubbles have vanished will be diluted by the expansion. Suppose we consider the physical number density  $n_b$  at time  $\eta$ , then

$$n_b(\eta) = \left( \frac{a(\eta_f)}{a(\eta)} \right)^3 \frac{\beta^3}{8\pi v_w^3}. \quad (3.49)$$

The corresponding physical mean bubble separation would be

$$R_*(\eta) = \frac{a(\eta)}{a(\eta_f)} (8\pi)^{1/3} \frac{v_w}{\beta(v_w)}. \quad (3.50)$$

Therefore the relation between  $R_*$  and  $\beta$  is similar to that derived in Minkowski spacetime and needs only additional attention on the scale factors. If one uses  $R_{*c}$  and  $\beta_c$ , then the relation is exactly the same as in Minkowski spacetime. We emphasize again that  $\beta$  and  $\beta_c$  are functions of  $v_w$ . To see this, we plot  $R_*$  at a time immediately after all the bubbles have disappeared, as a function of  $v_w$ , in the left panel of Fig. 8. For each  $v_w$ , we can find the corresponding  $\beta(v_w)$  as implied in above equation and compare with  $\beta(v_w)$  directly calculated using Eq. 3.47. This comparison is shown in the right panel and the two different determinations differ by at most 2%, where the uncertainty can be attributed to the approximations made.

#### 4 Fluid Velocity Field and Power Spectrum

The dominant source of gravitational wave production is the sound waves in a perturbed plasma due to the advancing bubble walls and their interaction with the surrounding fluid. In the sound shell model [42, 43], the total velocity field is modelled as a linear superposition of the individual contribution from each bubble. The first step is then to understand the velocity profile of the fluid around a single bubble. This topic has been extensively studied several decades ago and is reviewed

with a complete treatment in Ref. [41]. However the analysis is set in Minkowski spacetime and it is not clear whether it needs changes in an expanding universe. Ref. [85] studied the velocity profile in an expanding universe and found that there is a significant change to the velocity profile and a reduction of energy fraction going into the kinetic energy of the sound waves. But we will see in this section the velocity profile actually remains unchanged. We first review the full set of fluid and field equations and then analyze the fluid velocity profile around a single bubble. Armed with this information, we then find the total velocity field from a population of bubbles in the sound shell model and calculate the velocity field power spectrum.

#### 4.1 Fluid and Field Equations

Numerical simulations that are performed to provide the widely adopted gravitational wave formulae are based on the fluid-order parameter field model [39, 86, 87] in Minkowski spacetime. Here we generalize the full set of equations used in the simulations to the FLRW universe. Our purpose is to understand whether simulations can be done in Minkowski spacetime and then generalized to an expanding universe by simple rescalings of the physical quantities. This is an important question as it is computationally very expensive to do a numerical simulation.

The universe consists of: (1) the underlying scalar field(s) responsible for the phase transition; (2) the relativistic plasma whose constituent particles can interact with the scalar field(s); (3) magnetic field produced from the phase transition; (4) other sectors which do not directly interact with either the scalar field, the plasma or the magnetic field, though they do interact gravitationally. We will neglect (3) by focusing on the dominant source for gravitational wave production, and only consider (4) through its effect on the expansion. Given our cosmological context, the total energy momentum tensor for (1) and (2) is given by [39]

$$T^{\mu\nu} = \partial^\mu \phi \partial^\nu \phi - \frac{1}{2} g^{\mu\nu} \partial_\mu \phi \partial^\mu \phi + (e + p) U^\mu U^\nu + g^{\mu\nu} p, \quad (4.1)$$

where  $U^\mu = \gamma(1, \mathbf{v}/a)$  with  $\gamma = 1/\sqrt{1-v^2}$  and  $\mathbf{v} = d\mathbf{x}/d\eta$ . The energy and momentum density are given by

$$\begin{aligned} e &= a_B T^4 + V(\phi, T) - T \frac{\partial V}{\partial T}, \\ p &= \frac{1}{3} a_B T^4 - V(\phi, T), \end{aligned} \quad (4.2)$$

where  $a_B = g_* \pi^2/30$  and  $g_*$  is the relativistic degrees of freedom. It is certainly conserved, i.e.,  $T^{\mu\nu}_{;\mu} = 0$ <sup>3</sup>, and it is split into two parts by adding and subtracting a friction term  $\delta^\nu$  [86]:

$$\begin{aligned} T^{\mu\nu}_{;\mu}|_{\text{field}} &= (\partial^2 \phi) \partial^\nu \phi + \frac{1}{\sqrt{g}} (\partial_\mu \sqrt{g}) (\partial^\mu \phi) (\partial^\nu \phi) - \frac{\partial V}{\partial \phi} \partial^\nu \phi = \delta^\nu, \\ T^{\mu\nu}_{;\mu}|_{\text{fluid}} &= \partial_\mu [(e + p) U^\mu U^\nu] + \left[ \frac{1}{\sqrt{g}} (\partial_\mu \sqrt{g}) g^\nu_\lambda + \Gamma^\nu_{\mu\lambda} \right] (e + p) U^\mu U^\lambda + g^{\mu\nu} \partial_\mu p + \frac{\partial V}{\partial \phi} \partial^\nu \phi = -\delta^\nu. \end{aligned} \quad (4.3)$$

Note here the appearance of  $\partial_\mu g$  and  $\Gamma^\nu_{\mu\lambda}$  as we are using a generic metric. The friction term  $\delta^\nu$  is modelled by  $\delta^\nu = \eta U^\mu \partial_\mu \phi \partial^\nu \phi$ . For high temperatures it can be chosen as  $\eta = \tilde{\eta} \phi^2/T$  [40], which works well in that case [88] but may lead to numerical singularities for small temperature. The

<sup>3</sup>The subscript “;” denotes covariant derivative.

numerical simulations on sound waves adopted a constant value for the lower temperature case [89]. The exact set of equations can also be derived from field theory [83, 90].

In an FLRW universe, the field energy momentum conservation leads to a scalar equation:

$$-\ddot{\phi} + \frac{1}{a^2} \nabla^2 \phi - \frac{\partial V}{\partial \phi} - 3 \frac{\dot{a}}{a} \dot{\phi} = \eta \gamma (\dot{\phi} + \frac{1}{a} \mathbf{v} \cdot \nabla \phi), \quad (4.4)$$

which is just the Klein-Gordon equation for the scalar field when the friction term is absent, i.e., when  $\eta = 0$ . The vector part of the fluid energy-momentum conservation gives:

$$\dot{Z}^i + \frac{1}{a} \nabla \cdot (\mathbf{v} Z^i) + 5 \frac{\dot{a}}{a} Z^i + \frac{1}{a^2} \partial_i p + \frac{1}{a^2} \frac{\partial V}{\partial \phi} \partial_i \phi = -\frac{1}{a^2} \eta \gamma (\dot{\phi} + \frac{1}{a} \mathbf{v} \cdot \nabla \phi) \partial_i \phi, \quad (4.5)$$

where  $Z^i \equiv \gamma(e+p)U^i = \gamma^2(e+p)v^i/a$ . The parallel projection along  $U_\nu$  for the fluid gives another scalar equation:

$$\begin{aligned} \dot{E} + p[\dot{\gamma} + \frac{1}{a} \nabla \cdot (\gamma \mathbf{v})] + \frac{1}{a} \nabla \cdot (E \mathbf{v}) - \gamma \frac{\partial V}{\partial \phi} (\dot{\phi} + \frac{1}{a} \mathbf{v} \cdot \nabla \phi) + 3 \frac{\dot{a}}{a} \gamma (e+p) \\ = \eta \gamma^2 (\dot{\phi} + \frac{1}{a} \mathbf{v} \cdot \nabla \phi)^2, \end{aligned} \quad (4.6)$$

where  $E \equiv e\gamma$ . While the above equations form a complete set, the velocity profile is usually derived from a different scalar equation, the perpendicular projection for the fluid along the direction  $\bar{U}_\nu$ , which is defined by

$$\bar{U}^\mu U_\mu = 0, \quad \bar{U}^\mu \bar{U}_\mu = 1, \quad (4.7)$$

and takes the explicit form  $\bar{U}^\mu = \gamma(v, \hat{v}^i/a)$ . This gives

$$\begin{aligned} \left[ \frac{\dot{a}}{a} v + \gamma^2 \left( \dot{v} + \frac{1}{2a} \hat{\mathbf{v}} \cdot \nabla v^2 \right) \right] (e+p) + v \dot{p} + \frac{1}{a} \hat{\mathbf{v}} \cdot \nabla p + \frac{\partial V}{\partial \phi} (v \dot{\phi} + \frac{1}{a} \hat{\mathbf{v}} \cdot \nabla \phi) \\ = -\eta \gamma (v \dot{\phi} + \frac{1}{a} \hat{\mathbf{v}} \cdot \nabla \phi) (\dot{\phi} + \frac{1}{a} \mathbf{v} \cdot \nabla \phi). \end{aligned} \quad (4.8)$$

These equations are direct generalizations of those in Ref. [39] to an FLRW universe. It is not possible, however, to express the above equations in a form used in Minkowski spacetime and the problem lies with the scalar field. Despite this, the effect on the bubble and fluid motions should be minor, since the bubble collision process is fast compared with the long duration of the ensuing sound waves.

The process of the phase transition can thus be divided into two stages. The first stage is the bubble collision and disappearance of the symmetric phase, and the second is the propagation of sound waves. The difference between them is that the first stage takes a much shorter time, while the second is long-lasting. This is indeed what is observed from numerical simulations and should well justify simply neglecting the change of the scale factor during the first stage [39]. In this sense, the numerical simulations as performed in Ref. [39, 40] still give a faithful account of the first step for an expanding universe. However we will see in the next subsection that the analytical modelling of this first stage still admits simple rescaling properties and takes the same form as in Minkowski.

During the second stage gravitational waves are dominantly produced due to the long-lasting nature of the sound waves. Therefore the change of the scale factor cannot be ignored. The question is: can we still only perform numerical simulations in Minkowski spacetime. Fortunately, during this stage, the scalar field plays no dynamical role and we can consider only the fluid. The corresponding

equations can indeed be reduced to the Minkowski form. This is achieved by using the conformal time, neglecting the scalar field as well as the friction terms and using  $p = e/3$  for the plasma. Then Eq. 4.5, Eq. 4.6 and Eq. 4.8 reduce to (again,  $t \equiv \partial/\partial\eta$ ):

$$\begin{aligned} (a^4 S^i)' + \nabla \cdot (a^4 S^i \mathbf{v}) + \partial_i (a^4 p) &= 0, \\ (a^4 e \gamma)' + [\gamma' + \nabla \cdot (\gamma \mathbf{v})] (a^4 p) + \nabla \cdot (a^4 e \gamma \mathbf{v}) &= 0, \\ \gamma^2 (v' + \frac{1}{2} \hat{\mathbf{v}} \cdot \nabla v^2) [a^4 (e + p)] + v (a^4 p)' + \hat{\mathbf{v}} \cdot \nabla (a^4 p) &= 0, \end{aligned} \quad (4.9)$$

where  $S^i = aZ^i = \gamma^2 (e + p) v^i$ . The Minkowski counterpart of these equations can be obtained by setting  $a = 1$ . This suggests that we can define rescaled quantities  $\tilde{e} = a^4 e$  and  $\tilde{p} = a^4 p$ , which are free from the dilution due to the expansion, and that the equations governing  $\tilde{e}$ ,  $\tilde{p}$  and  $v$  take exactly the same form as their Minkowski counterparts, as long as the time  $t$  is interpreted as the conformal time  $\eta$ . We will see how these rescaled quantities can be used to derive the modified gravitational wave spectrum in later sections.

We note here that these equations were derived earlier in Ref. [91, 92] when also considering electromagnetism and it was shown that the above rescaling works not only for the purely fluid system but also for a system containing both fluid and electromagnetism. Including electromagnetism will add additional terms to the right hand side of the above equations.

## 4.2 Velocity Profile around a Single Bubble

Solving the velocity profile for a single expanding bubble depends on analyzing the behavior of the system consisting of both the fluid and the scalar field. This is usually done in the so called bag equation of state model, as summarized in Ref. [41]. The energy momentum tensor for the fluid plus scalar field system is assumed to take the following form (“+” for outside the bubble and “−” for inside):

$$T_{\pm}^{\mu\nu} = p_{\pm} g^{\mu\nu} + (p_{\pm} + \rho_{\pm}) U^{\mu} U^{\nu}, \quad (4.10)$$

with the bag equation of state:

$$\begin{aligned} p_+ &= \frac{1}{3} a_+ T_+^4 - \epsilon, & e_+ &= a_+ T_+^4 + \epsilon. \\ p_- &= \frac{1}{3} a_- T_-^4, & e_- &= a_- T_-^4, \end{aligned} \quad (4.11)$$

where  $\epsilon$  is the vacuum energy difference between the false and true vacua. One can also find the enthalpy  $\omega = e + p$ . Here  $v$ ,  $T$  and thus  $e, p, \omega$  all vary from the bubble center to the region far outside the bubble where there is no perturbation. The task is to solve for these fields at regions both inside and outside the bubbles and smoothly match these two sets of solutions through the junction conditions across the bubble wall.

### 4.2.1 Inside the Bubble

In this region, we drop all terms related to  $\phi$  including the vacuum energy from  $\epsilon$ , and we also apply the relation  $p = e/3$ <sup>4</sup>. The resulting equations are already given in Eq. 4.9 and the equations are exactly the same as the Minkowski counterpart when the rescaled quantities are used. Now, assuming a spherically symmetric profile and denoting the comoving bubble radius with  $r$  and the conformal

<sup>4</sup>Of course, we are assuming a constant value of the speed of sound, i.e.,  $c_s = 1/\sqrt{3}$ . Without doing so, the equations cannot be put into the form in Eq. 4.9. We also dropped any spatial variation of the scalar field and its time variation following the conventional analysis.

time elapsed since its nucleation as  $\Delta\eta$ , the solution should be a self-similar one which depends solely on the ratio  $\xi \equiv r/\Delta\eta$ . Then we can obtain the same equations as in Minkowski spacetime:

$$\begin{aligned}(\xi - v)\partial_\xi \tilde{e} &= \tilde{w} \left[ 2\frac{v}{\xi} + \gamma^2(1 - \xi v)\partial_\xi v \right], \\(1 - v\xi)\partial_\xi \tilde{p} &= \tilde{w}\gamma^2(\xi - v)\partial_\xi v,\end{aligned}\tag{4.12}$$

which can then be combined to give an equation for the velocity field:

$$2\frac{v}{\xi} = \gamma^2(1 - v\xi) \left[ \frac{\mu^2}{c_s^2} - 1 \right] \partial_\xi v.\tag{4.13}$$

Here  $\mu(\xi, v) = (\xi - v)/(1 - \xi v)$ , which is the Lorentz boost transformation. This equation can be directly solved given a boundary condition at the wall, to be specified later.

#### 4.2.2 Outside the Bubble

Outside the bubble, the presence of the constant vacuum energy term  $\epsilon$  seemingly does not allow us to reach Eq. 4.9 for two possible reasons: (1) we can not apply  $p = e/3$  since  $p = -e$  for vacuum energy; (2)  $\epsilon$  does not scale like radiation with the behavior  $1/a^4$  and the rescaled quantity  $a^4 e$  still contains the expansion effect. Let us look more closely at the equations. The parallel projection in Eq. 4.6, when the friction and scalar gradient terms are neglected, becomes

$$\left[ (\gamma e)' + 3\frac{a'}{a}\gamma(e + p) \right] + p[\gamma' + \nabla \cdot (\gamma \mathbf{v})] + \nabla \cdot (\gamma e \mathbf{v}) = 0.\tag{4.14}$$

Correspondingly, the perpendicular projection in Eq. 4.8 reduces to

$$\left[ \frac{a'}{a}v(e + p) + vp' \right] + \gamma^2(v' + \frac{1}{2}\hat{\mathbf{v}} \cdot \nabla v^2)(e + p) + \hat{\mathbf{v}} \cdot \nabla p = 0.\tag{4.15}$$

In the absence of the vacuum energy inside  $e$  and  $p$ , both of above equations can be put into the form in Eq. 4.9, by combining the terms in  $[\dots]$  and using  $e = 3p$ . The resulting equations for the rescaled quantities are the same as in Minkowski spacetime. The presence of  $\epsilon$  makes this impossible. In Ref. [85], the self-similar velocity profile is assumed anyway. But the existence of an explicit time dependence from  $a'$  makes it impossible to solve, except in corners of the parameter space where it vanishes numerically. It is also in doubt if there exists a self-similar solution at all for these equations and we refrain from going in that direction.

Despite this dilemma, we can still cast above equations in the form 4.9 under the assumption that  $\epsilon$  is a constant of time during this very short period of time. Then the first equation can be reorganized in the following way:

$$\left[ \gamma' + \nabla \cdot (\gamma \mathbf{v}) + 3\frac{a'}{a}\gamma \right] (e + p) + \gamma e' + \gamma \mathbf{v} \cdot \nabla e = 0.\tag{4.16}$$

Then  $\epsilon$  cancels out in  $(e + p)$  and drops out in  $e'$ , and of course also in  $\nabla e$ . So above  $e$  and  $p$  can include only the fluid part. Then one can put it back into the previous form 4.14 and define the rescaled quantities:  $\tilde{e}$ ,  $\tilde{p}$ , which obey exactly the same equation as in the Minkowski spacetime. Therefore we obtain the second equation in Eq. 4.9 and the first in Eq. 4.12. Similarly for Eq. 4.15,  $\epsilon$  drops out in all terms and one can safely define the rescaled quantities, and obtain the third equation in Eq. 4.9 and the second in Eq. 4.12. Combining these two equations again gives the same equation for the velocity field as in Eq. 4.13.



### 4.2.3 Matching at Bubble Wall

The equation 4.13 for both regions needs the junction conditions at the wall to connect them. They are derived by integrating the conservation of energy momentum tensor across the bubble wall, which gives in the wall frame (note  $+$ ,  $-$  denote quantities at positions immediately outside and inside the wall) <sup>5</sup>

$$T_+^{r\eta} = T_-^{r\eta}, \quad (4.17)$$

$$T_+^{rr} = T_-^{rr}, \quad (4.18)$$

where  $v_-$  and  $v_+$  are both at wall frame. These two equations imply

$$(e_+ + p_+)v_+\gamma_+^2 = (e_- + p_-)v_-\gamma_-^2, \quad (4.19)$$

$$(e_+ + p_+)v_+^2\gamma_+^2 + p_+ = (e_- + p_-)v_-^2\gamma_-^2 + p_-. \quad (4.20)$$

Here both  $e_{\pm}$  and  $p_{\pm}$  are the ordinary energy density and pressure and include the vacuum energy  $\epsilon$ . The reason is while they can be neglected away from the bubble wall due to the vanishing spatial gradient, they jump across the bubble wall and give non-negligible contributions to the above equations. The junction equations can be solved by making the change of variables  $v = \tanh(\phi)$  and  $\gamma^2 = \cosh^2(\phi)$  which, after simplifying, will yield two linear equations in  $\cosh^2(\phi_+)$  and  $\cosh^2(\phi_-)$ . The solution will give

$$v_+ = \sqrt{\frac{(p_- - p_+)(e_- + p_+)}{(e_- - e_+)(e_+ + p_-)}},$$

$$v_- = \sqrt{\frac{(p_+ - p_-)(e_+ + p_-)}{(e_+ - e_-)(e_- + p_+)}}. \quad (4.21)$$

The product and ratio of  $v_+$  and  $v_-$  can further be found,

$$v_+v_- = \frac{p_+ - p_-}{e_+ - e_-}, \quad \frac{v_+}{v_-} = \frac{e_- + p_+}{e_+ + p_-}. \quad (4.22)$$

Plugging  $e_{\pm}, p_{\pm}$  as specified by the bag equation of state in Eq. 4.11 leads to

$$v_+v_- = \frac{1 - (1 - 3\alpha_+)\sigma}{3 - 3(1 + \alpha_+)\sigma}, \quad (4.23)$$

$$\frac{v_+}{v_-} = \frac{3 + (1 - 3\alpha_+)\sigma}{1 + 3(1 + \alpha_+)\sigma}, \quad (4.24)$$

where  $\alpha_+$  and  $\sigma$  are defined by

$$\alpha_+ = \frac{\epsilon}{a_+T_+^4} \Big|_{\text{wall}}, \quad \sigma = \frac{a_+T_+^4}{a_-T_-^4} \Big|_{\text{wall}}. \quad (4.25)$$

$\alpha_+$  characterizes the amount of vacuum energy released from the phase transition normalized by the total radiation energy density immediately outside the bubble (as denoted by the subscript ‘‘wall’’). It is not the  $\alpha$  usually used in phase transition analyses. Rather, its value should be solved from the

<sup>5</sup> Also we follow the conventional procedure by neglecting the time dependence of the various quantities.

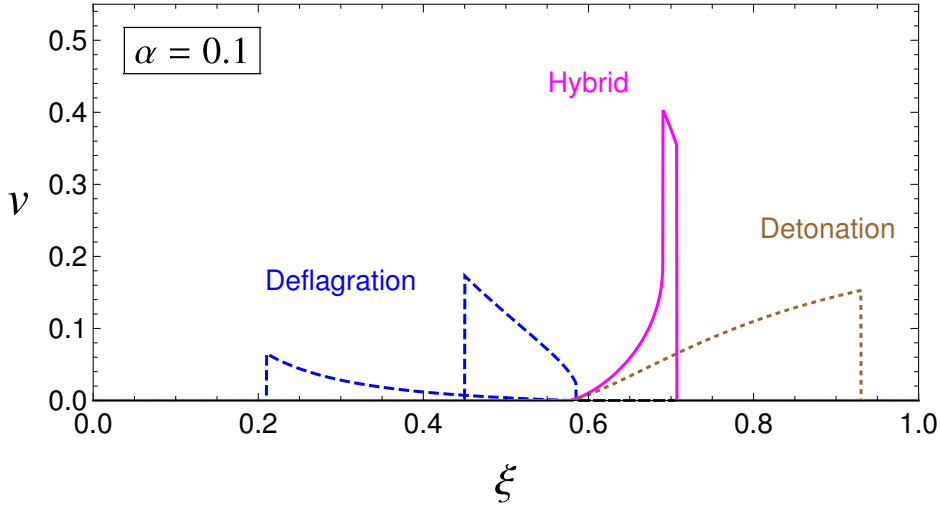


**Figure 9.** Representative velocity profiles surrounding the bubble walls.

requirement that far from the bubble where the plasma is not perturbed (denote by  $\infty$ ), the corresponding  $\alpha_+$  at  $\infty$  matches  $\alpha$ . The two equations in Eq. 4.24 can be solved for both  $r$  and  $v_+$  to give two branch solutions for the velocity in the symmetric phase,

$$v_+ = \frac{1}{1 + \alpha_+} \left[ \left( \frac{v_-}{2} + \frac{1}{6v_-} \right) \pm \sqrt{\left( \frac{v_-}{2} + \frac{1}{6v_-} \right)^2 + \alpha_+^2 + \frac{2}{3}\alpha_+ - \frac{1}{3}} \right]. \quad (4.26)$$

Up to this point, the results for the velocity profile are exactly the same as in Minkowski space-time, but with the understanding that the time  $t$  is replaced by the conformal time  $\eta$ ,  $v = dx/d\eta$  and  $(e, p)$  are replaced by  $(\tilde{e}, \tilde{p})$ . We will not go into the details of the physics of above results but only summarize the main features of the velocity profile relevant for this study and refer the reader to Ref. [41] for a more detailed analysis.

The fluid admits three modes of motion: deflagration, detonation and supersonic deflagration (also called hybrid) [93], with representative velocity profiles shown in Fig. 9. For deflagration, the velocity inside the bubble vanishes and is only non-zero outside. Detonation is the opposite, with non-zero velocity inside the bubble. Supersonic deflagration has non-zero velocity both inside and outside the bubble. Therefore for deflagration,  $v_- = v_w$  which should be used in Eq. 4.26 to find  $v_+$ , choosing a value of  $\alpha_+$ . This  $v_+$  is Lorentz transformed to the plasma static frame to find  $v(v_w)$  immediately outside the wall, which is then used as the boundary condition to solve for  $v(\xi)$  outside the wall. It might not consistently drop to zero, in which case a shock front is encountered and should be determined. Beyond the shock  $v(\xi) = 0$ . This gives a complete profile, but not yet the correct one, since a specific value of  $\alpha_+$  is used in above determination of the profile. This value needs to be tuned such that  $\alpha_+ = \alpha$  far outside the bubble. For detonation,  $v_+ = v_w$  and  $v_-$  can be determined from Eq. 4.26 with  $\alpha_+ = \alpha$  as outside the bubble the plasma is not perturbed. Then one can Lorentz transform  $v_-$  to  $v(v_w)$  immediately inside the wall and use it as a boundary condition to determine the full profile. No inconsistency or shock front will be encountered in this case. For supersonic deflagration, the condition  $v_- = c_s$  is the boundary condition used. Shock front can exist in this case and should be treated similarly. We refer the reader for more details in Ref. [41].

### 4.3 Velocity Field in the Sound Shell Model

With the velocity profile surrounding a single bubble determined, we can now find the total velocity field, as needed in Eq. 2.19. As we have already seen, in an expanding universe the equations of motion of the fluid are exactly the same as those in non-expanding Minkowski spacetime. This means that the equation of motion for the sound waves remain the same as its Minkowski counterpart, as long as we replace  $t$  by  $\eta$  and interpret the velocity as obtained by differentiation with respect to the conformal time. So the procedure parallels that in Ref. [43].

Lets start with the contribution from one bubble. Before it collides with another bubble, the velocity profile is governed by equations given in previous sections. After the collision, the friction vanishes and the velocity field starts freely propagating and becomes sound waves, with the speed of sound  $c_s$ . So we need to match the velocity profile surrounding this bubble with the velocity field at the time when the friction vanishes. Before collision, we can Fourier decompose the velocity field as

$$v^i(\eta < \eta_{fc}, \mathbf{x}) = \frac{1}{2} \int \frac{d^3q}{(2\pi)^3} [\tilde{v}_{\mathbf{q}}^i(\eta) e^{i\mathbf{q}\cdot\mathbf{x}} + \tilde{v}_{\mathbf{q}}^{i*}(\eta) e^{-i\mathbf{q}\cdot\mathbf{x}}], \quad (4.27)$$

with  $\mathbf{x}$  being the comoving coordinate and  $\mathbf{q}$  the comoving wavenumber. After collision, the velocity field freely propagates as sound waves and admits the following decomposition:

$$v^i(\eta, \mathbf{x}) = \int \frac{d^3q}{(2\pi)^3} [v_{\mathbf{q}}^i e^{-i\omega\eta + i\mathbf{q}\cdot\mathbf{x}} + v_{\mathbf{q}}^{i*} e^{i\omega\eta - i\mathbf{q}\cdot\mathbf{x}}]. \quad (4.28)$$

where  $\omega = qc_s$ . Since the plasma consists of relativistic particles,  $c_s = 1/\sqrt{3}$ . Here  $v_{\mathbf{q}}^i$  is independent of  $\eta$ , different from  $\tilde{v}_{\mathbf{q}}^i(\eta)$ .

The task is then to find the contribution to  $v_{\mathbf{q}}^i$  from  $\tilde{v}_{\mathbf{q}}^i(\eta)$  at  $\eta_{fc}$ . Since the equation governing the sound waves is of second order, we need the following initial conditions:  $\tilde{v}_{\mathbf{q}}^i(\eta)$  and  $\tilde{v}_{\mathbf{q}}^{i'}(\eta)$  at  $\eta_{fc}$ . While one can obtain  $\tilde{v}_{\mathbf{q}}^i(\eta)$  directly from the velocity profile in the previous section, one subtlety appears here for  $\tilde{v}_{\mathbf{q}}^{i'}(\eta)$ . As demonstrated in Ref. [43], the equation governing  $\tilde{v}_{\mathbf{q}}^{i'}(\eta)$  before the collision relies on a force term from the scalar field, which disappears once the collision occurs. So the value  $\tilde{v}_{\mathbf{q}}^{i'}(\eta)$  calculated with this force (as was previously used in Ref. [42]) is different from the corresponding value without it. It is the latter one that should enter the initial conditions for the sound waves. In this case, rather than calculating  $\tilde{v}_{\mathbf{q}}^{i'}(\eta)$  from the velocity profile  $\tilde{v}_{\mathbf{q}}^i(\eta)$ , we need to calculate it directly from the energy fluctuations:

$$\lambda(x) = \frac{\tilde{e}(x) - \bar{e}}{\bar{\omega}}, \quad (4.29)$$

where a bar denotes averaged quantity and tilde denotes rescaled quantity. Similarly its Fourier component  $\tilde{\lambda}_{\mathbf{q}}$  can be defined in analogy to Eq. 4.27, The equation for sound waves then follows:

$$\begin{aligned} \tilde{\lambda}_{\mathbf{q}}' + iq^j \tilde{v}_{\mathbf{q}}^j &= 0, \\ \tilde{v}_{\mathbf{q}}^{j'} + c_s^2 iq^j \tilde{\lambda}_{\mathbf{q}} &= 0. \end{aligned} \quad (4.30)$$

Therefore  $\tilde{v}_{\mathbf{q}}^{j'} = -c_s^2 iq^j \tilde{\lambda}_{\mathbf{q}}$ , and one needs to calculate  $v^i(\eta, \mathbf{x})$  and  $\lambda(\eta, \mathbf{x})$  from the self-similar velocity profile for one bubble. In coordinate space, the velocity profile for the  $n$ -th bubble can be written as

$$\mathbf{v}^{(n)}(\eta, \mathbf{x}) = \hat{\mathbf{R}}(\mathbf{x})v(\xi), \quad (4.31)$$

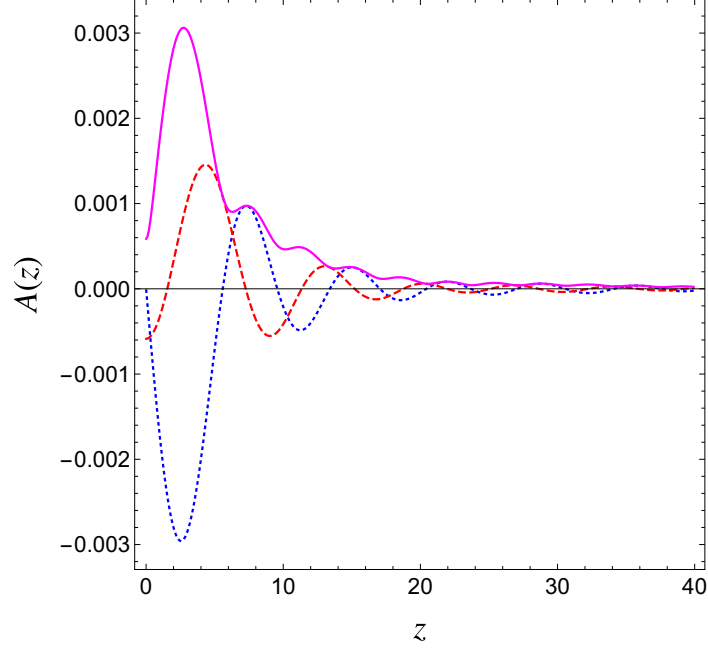


**Figure 10.** The real (blue dotted), imaginary (red dashed) parts and absolute value (magenta solid) of  $A(z)$  (defined below Eq. 4.35) for  $v_w = 0.92$  and  $\alpha = 0.0046$ .

where  $\mathbf{R}(\mathbf{x}) \equiv \mathbf{x} - \mathbf{x}^{(n)}$ ,  $\xi \equiv |\mathbf{R}^{(n)}|/T^{(n)}$  and  $T^{(n)}(\eta) \equiv \eta - \eta^{(n)}$ , with  $\mathbf{x}^{(n)}$  and  $\eta^{(n)}$  the coordinate of the bubble center and the conformal time when the bubble is nucleated. Similarly for  $\lambda$ , as it is a scalar field, we can define  $\lambda(\eta, \mathbf{x}) \equiv \lambda(\xi)$ . With the profile specified in coordinate space, the corresponding Fourier coefficients can be obtained straightforwardly

$$\begin{aligned}\tilde{v}_{\mathbf{q}}^{j(n)}(\eta_{fc}) &= e^{-i\mathbf{q}\cdot\mathbf{x}^{(n)}} (T^{(n)})^3 i\hat{z}^j f'(z)|_{\eta=\eta_{fc}}, \\ \tilde{\lambda}_{\mathbf{q}}^{(n)}(\eta_{fc}) &= e^{-i\mathbf{q}\cdot\mathbf{x}^{(n)}} (T^{(n)})^3 l(z)|_{\eta=\eta_{fc}},\end{aligned}\quad (4.32)$$

with  $\mathbf{z} \equiv \mathbf{q}T^{(n)}$  and the two functions  $f(z)$  and  $l(z)$  given by

$$\begin{aligned}f(z) &= \frac{4\pi}{z} \int_0^\infty d\xi v(\xi) \sin(z\xi), \\ l(z) &= \frac{4\pi}{z} \int_0^\infty d\xi \xi \lambda(\xi) \sin(z\xi).\end{aligned}\quad (4.33)$$

Then the  $n$ -th bubble's contribution to the Fourier coefficient of the sound waves is

$$v_{\mathbf{q}}^{j(n)} = \frac{1}{2} \left[ \tilde{v}_{\mathbf{q}}^{j(n)}(\eta_{fc}) + c_s \hat{q}^j \tilde{\lambda}_{\mathbf{q}}^{(n)}(\eta_{fc}) \right] e^{i\omega\eta_{fc}}, \quad (4.34)$$

and after using the explicit expression of the bubble profile,

$$v_{\mathbf{q}}^{j(n)} = i\hat{z}^j (T_{fc}^{(n)})^3 e^{i\omega\eta_{fc} - i\mathbf{q}\cdot\mathbf{x}^{(n)}} A(z_{fc}), \quad (4.35)$$

where  $A(z_{fc}) = [f'(z_{fc}) - ic_s l(z_{fc})]/2$ , with an example shown in Fig. 10. Thus we have calculated the contribution to  $v_{\mathbf{q}}^i$  from one bubble that is nucleated randomly. The randomness of this bubble is

reflected in its formation time, location, collision time and its radius. Since the radius at collision is fixed once its formation and collision times are given, we have three independent random variables.

The velocity field after all bubbles have disappeared, can be assumed to be the linear addition of the contributions from all bubbles, which is the essence of the sound shell model [42, 43]. Suppose the total number of bubbles nucleated within a Hubble volume with comoving size  $V_c$  is  $N_b$ . Then the velocity field can be assumed, according to the sound shell model, to be given by

$$v_{\mathbf{q}}^i = \sum_{n=1}^{N_b} v_{\mathbf{q}}^{i(n)}. \quad (4.36)$$

#### 4.4 Velocity Power Spectrum

As these  $N_b$  bubbles are just one realization of the phase transition, the resulting  $v_{\mathbf{q}}^i$  has a random nature with it and follows a Gaussian distribution to a good approximation according to the central limit theorem<sup>6</sup>. Randomness of this kind can be removed by doing an ensemble average of the product:  $\langle v_{\mathbf{q}}^i v_{\mathbf{q}}^{j*} \rangle$ , which is all needed for a Gaussian distribution. Now let us see how this is achieved.

The  $N_b$  bubbles can be separated into groups with the bubbles within each group sharing a common formation and collision time. Then the only variable that is random across the bubbles of one group, e.g., group  $g$  with  $N_g$  bubbles, is the spatial locations of the bubbles when they form. Now consider group  $g$ . Its contribution to the correlator is

$$\langle v_{\mathbf{q}_1}^i v_{\mathbf{q}_2}^{j*} \rangle_g = \tilde{q}_1^i \tilde{q}_2^j [T_{fc}^{(g)}]^6 A(z_{fc}^{(n)}) A(z_{fc}^{(m)})^* e^{i(\omega_1 - \omega_2) \eta_{fc}^{(g)}} \left\langle \sum_{m,n=1}^{N_g} e^{i\mathbf{q}_2 \cdot \mathbf{x}^{(m)} - i\mathbf{q}_1 \cdot \mathbf{x}^{(n)}} \right\rangle. \quad (4.37)$$

Here the order of the ensemble average and the summation can be switched. Since the ensemble average of each of these  $N_g$  terms gives the same result and oscillatory cross terms vanish, we have

$$\begin{aligned} \left\langle \sum_{m,n=1}^{N_g} e^{i\mathbf{q}_2 \cdot \mathbf{x}^{(m)} - i\mathbf{q}_1 \cdot \mathbf{x}^{(n)}} \right\rangle &= N_g \delta_{mn} \langle e^{i\mathbf{q}_2 \cdot \mathbf{x}^{(m)} - i\mathbf{q}_1 \cdot \mathbf{x}^{(n)}} \rangle \\ &= N_g \frac{1}{V_c} \int d^3 \mathbf{x}^{(*)} e^{i(\mathbf{q}_2 - \mathbf{q}_1) \cdot \mathbf{x}^{(*)}} \\ &= N_g \frac{1}{V_c} (2\pi)^3 \delta^3(\mathbf{q}_1 - \mathbf{q}_2). \end{aligned} \quad (4.38)$$

The constraint  $\mathbf{q}_1 = \mathbf{q}_2$  removes the  $\eta_{fc}^{(g)}$  dependence, leading to a result solely dependent on the conformal lifetime of the bubble  $T_{fc}^{(g)} \equiv \eta_{lt}$  but not their absolute formation or destruction time:

$$\langle v_{\mathbf{q}_1}^i v_{\mathbf{q}_2}^{j*} \rangle_g = \tilde{q}_1^i \tilde{q}_2^j \eta_{lt}^6 |A(q\eta_{lt})|^2 \frac{N_g}{V_c} (2\pi)^3 \delta^3(\mathbf{q}_1 - \mathbf{q}_2). \quad (4.39)$$

This result means that we can combine groups with the same  $\eta_{lt}$ , and of course, different formation time, by solely enlarging the value of  $N_g$ . In the following we will simply stick to the group label “ $g$ ”, though its definition is changed and now includes all bubbles with the same  $\eta_{lt}$ . Restricting to a sufficiently small region centered at  $\eta_{lt}$ , the number  $N_g$  is still an infinitesimally small fraction of  $N_b$  and can be written as

$$N_g = N_b P(\eta_{lt}) d\eta_{lt}, \quad (4.40)$$

<sup>6</sup> If there is a sufficiently large population of bubbles within this single volume, the summation of these contributions can also remove the randomness, equivalent to an ensemble average.

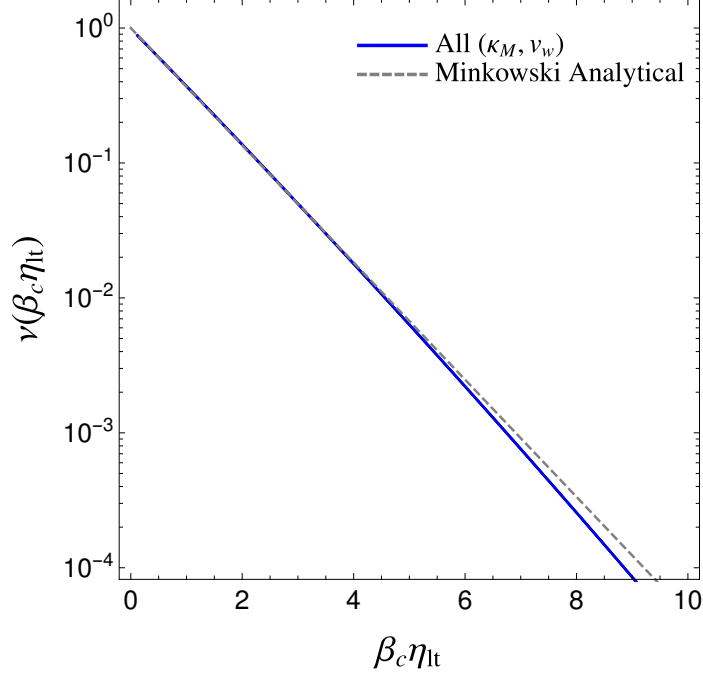


**Figure 11.** The dimensionless bubble lifetime distribution  $\nu(\beta_c \eta)$  defined in Eq. 4.45 and more explicitly in Eq. 4.47. All previously used choices of  $\kappa, v_w$  give the same blue line. The gray dashed line is the analytically derived result  $e^{-\beta t_h}$  in Ref. [43].

where  $P(\eta_{lt})$  is the probability density for bubbles to have conformal lifetime in the range  $(\eta_{lt}, \eta_{lt} + d\eta_{lt})$ , thus with dimension 1 and normalized by

$$\int d\eta_{lt} P(\eta_{lt}) = 1. \quad (4.41)$$

Adding the contributions from all the groups and noting that cross terms vanish due to the oscillatory behavior, we have

$$\langle v_{\mathbf{q}_1}^i v_{\mathbf{q}_2}^{j*} \rangle = \hat{q}_1^i \hat{q}_2^j (2\pi)^3 \delta^3(\mathbf{q}_1 - \mathbf{q}_2) \int d\eta_{lt} \left[ P(\eta_{lt}) \frac{N_b}{V_c} \right] \eta_{lt}^6 |A(q\eta_{lt})|^2. \quad (4.42)$$

One can now identify the quantity in the square bracket as the conformal lifetime distribution defined in Eq. 3.29:

$$P(\eta_{lt}) \frac{N_b}{V_c} = \tilde{n}_{b,c}(\eta_{lt}). \quad (4.43)$$

Since  $P(\eta_{lt})$  is of dimension 1, it is convenient to define a dimensionless version of it  $\nu$ :

$$P(\eta_{lt}) \equiv \beta_c \nu(\beta_c \eta_{lt}). \quad (4.44)$$

Then

$$\tilde{n}_{b,c}(\eta_{lt}) = \frac{\beta_c}{R_{*c}^3} \nu(\beta_c \eta_{lt}), \quad (4.45)$$

with  $R_{*c}$  is the asymptotic comoving mean bubble separation. Then we have

$$\langle v_{\mathbf{q}_1}^i v_{\mathbf{q}_2}^{j*} \rangle = \hat{q}_1^i \hat{q}_2^j (2\pi)^3 \delta^3(\mathbf{q}_1 - \mathbf{q}_2) \underbrace{\frac{1}{R_{*c}^3 \beta_c^6} \int d\tilde{T} \tilde{T}^6 \nu(\tilde{T}) |A(\frac{q\tilde{T}}{\beta_c})|^2}_{\equiv P_v(q)}, \quad (4.46)$$

with here  $\tilde{T} = \beta_c \eta_t$ , and we have defined the spectral density  $P_v(q)$  for the plane wave amplitude  $v_{\mathbf{q}}^i$ . Lets write down the explicit expression for  $\nu(\tilde{T})$ . From Eq. 4.45 and 3.29, we have

$$\nu(\tilde{T}) = v_w R_{*c}^3 \int_{t_c}^{t_f} dt' p(t') a^3(t') \frac{\mathcal{A}_c(t', v_w \tilde{T} / \beta_c)}{\beta_c}, \quad (4.47)$$

which can be directly used for numerical calculations once  $t'$  is transformed to  $T'$  as was done in previous sections. The numerically calculated distribution for the examples we have been using is shown in Fig. 11. For all choices of  $\kappa, v_w$ , the distributions are almost indistinguishable, shown as the blue curve, and it coincides with the gray dashed curve which denotes the distribution  $e^{-\tilde{T}}$ , derived analytically in Ref. [43]. With  $\nu(\tilde{T})$  obtained, the spectral density  $P_v(\tilde{T})$  can be calculated straightforwardly from its definition in Eq. 4.46.

To calculate the velocity power spectrum, we need to evaluate the correlator

$$\langle \tilde{v}_{\mathbf{q}}^i(\eta_1) \tilde{v}_{\mathbf{k}}^{j*}(\eta_2) \rangle = \delta^3(\mathbf{q} - \mathbf{k}) \hat{q}^i \hat{k}^j G(q, \eta_1, \eta_2), \quad (4.48)$$

and it can be shown that

$$G(q, \eta_1, \eta_2) = 2P_v(q) \cos[\omega(\eta_1 - \eta_2)]. \quad (4.49)$$

Plugging it into Eq. 2.21 or 2.22 gives the stress energy correlator. Also the velocity field power spectrum  $\mathcal{P}_v$  follows naturally,

$$\begin{aligned} \mathcal{P}_v &= \frac{q^3}{2\pi^2} [2P_v(q)] \\ &= \frac{1}{64\pi^4 v_w^6} (q R_{*c})^3 \int d\tilde{T} \tilde{T}^6 \nu(\tilde{T}) \left| A \left( \frac{(q R_{*c}) \tilde{T}}{(8\pi)^{1/3} v_w} \right) \right|^2, \end{aligned} \quad (4.50)$$

and we have used  $\beta_c R_{*c} = (8\pi)^{1/3} v_w$ . It is obvious to see that  $\mathcal{P}_v$  is dimensionless, as it is constructed with purely dimensionless quantities. A representative profile for the velocity power spectrum is shown in Fig. 12 assuming an exponential bubble nucleation rate, and more details about its properties can be found in Ref. [42].

## 5 Gravitational Wave Power Spectrum

We can now go back to Eq. 2.14 and collect all the pieces to calculate the gravitational power spectrum. It only remains to calculate the Green's function, and it requires to specify an expansion scenario. We will as usual focus on the RD and MD scenarios as examples, but the method here is applicable to any expansion history.

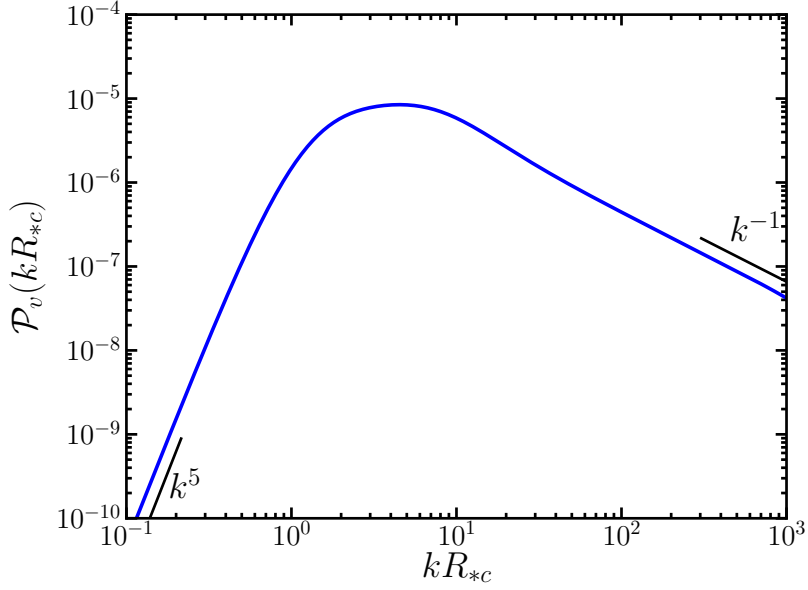


**Figure 12.** Representative velocity power spectrum for  $\alpha = 0.0046$  and  $v_w = 0.92$ . Velocity power spectrum calculated in the sound shell model for a weak phase transition with  $\alpha = 0.0046$  and  $v_w = 0.92$ . The bubbles were assumed to nucleate exponentially. The low and high frequency regimes follow the  $k^5$  and  $k^{-1}$  power law fits respectively (black solid lines).

## 5.1 Solutions in Radiation and Matter Domination

First, we choose a parameter to measure the time of the cosmic history. It can either be the actual time  $t$ , the conformal time  $\eta$ , the redshift  $z$  or the scale factor  $a$ . To present a result independent of the origin of the time coordinate, we choose the dimensionless scale factor ratio  $y \equiv a/a_s$ , giving then  $d/dt = \dot{a}/a_s d/dy$ . Here  $a_s$  is the time when the source, the sound waves, becomes active, so that  $y$  starts from 1. The Friedmann equation gives the relation between  $y$  and the conformal time

$$y = \frac{\kappa_M}{4} (a_s H_s)^2 (\eta - \eta_s)^2 + a_s H_s (\eta - \eta_s) + 1. \quad (5.1)$$

It is obvious that when  $\eta = \eta_s$ , we have  $y = 1$ . Also it does not matter how the origin of the conformal time is chosen as it only depends on  $\Delta\eta \equiv \eta - \eta_s$ . For RD, where  $\kappa_M \sim 0$ , we have  $y = a_s H_s (\eta - \eta_s) + 1$ . For MD, where  $\kappa_M \approx 1$ ,  $y = [\frac{1}{2} a_s H_s (\eta - \eta_s) + 1]^2$ . In the literature, it is usually approximated that  $a \propto \eta$  deep inside the radiation era or  $a \propto \eta^2$  deep inside the matter era. However we remain agnostic about when the phase transition happens and do not require it to start deep inside the radiation or matter era. Also the duration of the phase transition is very small compared with the conformal time, which makes such approximation quite crude. But our choice using  $y$  is free from above limitations and offers a more accurate description of phase transition process.

With  $y$ , the Hubble rate, when assuming the existence of both matter and radiation components, takes the following form

$$H = H_s \sqrt{\frac{\kappa_M}{y^3} + \frac{1 - \kappa_M}{y^4}}, \quad (5.2)$$

where  $\kappa_M$  is the matter fraction of the total energy density at  $t_s$ .



Switching from the conformal time  $\eta$  to  $y$  in Eq. 2.5, the Einstein equation becomes <sup>7</sup>:

$$(\kappa_M y + 1 - \kappa_M) \frac{d^2 h_q}{dy^2} + \left[ \frac{5}{2} \kappa_M + \frac{2(1 - \kappa_M)}{y} \right] \frac{dh_q}{dy} + \tilde{q}^2 h_q = \frac{16\pi G a(y)^2 \pi_q^T(y)}{(a_s H_s)^2}. \quad (5.3)$$

Here  $\tilde{q} \equiv q/(a_s H_s)$ , which characterizes the number of wavelengths contained within a Hubble radius at  $t_s$ . The Green's function can be found by solving the homogeneous version of this equation, together with a slightly modified boundary conditions compared with Eq. 2.11:

$$G(y \leq y_0) = 0, \quad \frac{\partial G(y, y_0)}{\partial y} \Big|_{\tilde{\eta}=\tilde{y}_0^+} = \frac{1}{\kappa_M y_0 + 1 - \kappa_M}. \quad (5.4)$$

The solution to the homogeneous equation is a linear combination of the hypergeometric function and Bessel functions. For the case of radiation domination  $\kappa_M \ll 1$  and matter domination  $\kappa_M \approx 1$ , the solutions take simpler forms that can be expressed in terms of elementary functions. For RD, the equation becomes simpler when expressed using the parameter  $\tilde{y}$ , defined by

$$\tilde{y} = y\tilde{q} = q(\eta - \eta_s) + \tilde{q} = \Delta\tilde{\eta} + \tilde{q}. \quad (5.5)$$

Then the Einstein equation becomes

$$\frac{d^2 h_q}{d\tilde{y}^2} + \frac{2}{\tilde{y}} \frac{dh_q}{d\tilde{y}} + h_q = \frac{16\pi G a(y)^2 \pi_q^T(y)}{q^2}. \quad (5.6)$$

The corresponding Green's function can be easily solved:

$$G(\tilde{y}, \tilde{y}_0) = \frac{\tilde{y}_0 \sin(\tilde{y} - \tilde{y}_0)}{\tilde{y}}. \quad (5.7)$$

For MD, the wave equation can be similarly simplified with

$$\tilde{y} = y\tilde{q}^2 = \left[ \frac{1}{2} \Delta\tilde{\eta} + \tilde{q} \right]^2. \quad (5.8)$$

Note this definition is different from that in the radiation dominated case. Then the Einstein equation becomes

$$\tilde{y} \frac{d^2 h_q}{d\tilde{y}^2} + \frac{5}{2} \frac{dh_q}{d\tilde{y}} + h_q = \frac{16\pi G a(\tilde{y})^2 \pi_q^T(\tilde{y})}{q^2}. \quad (5.9)$$

The homogeneous equation for  $h_q$  can be transformed into the Bessel equation for a different variable  $Z(\lambda)$  defined by  $h_q = (\lambda/2)^{-3/2} Z(\lambda)$  with  $\lambda = 2\sqrt{\tilde{y}}$ :

$$\lambda^2 Z''(\lambda) + \lambda Z'(\lambda) + \left[ \lambda^2 - \left( \frac{3}{2} \right)^2 \right] Z(\lambda) = 0. \quad (5.10)$$

The two independent solutions are the first and second kind Bessel functions both with order 3/2, which can all be expressed in elementary functions. Upon using the boundary conditions, the Green's

---

<sup>7</sup>We are using a simplified notation for  $h$  and  $\pi^T$

function is found to be <sup>8</sup> :

$$G(\tilde{y}, \tilde{y}_0) = \frac{(\lambda\lambda_0 + 1) \sin(\lambda - \lambda_0) - (\lambda - \lambda_0) \cos(\lambda - \lambda_0)}{\lambda^3/2}. \quad (5.12)$$

Finally in both cases, the gravitational wave amplitude is given by

$$h_{ij}(\tilde{y}, \mathbf{q}) = \int_{\tilde{y}_s}^{\tilde{y}} d\tilde{y}' G(\tilde{y}, \tilde{y}') \frac{16\pi G a (\tilde{y}')^2 \pi_{ij}^T(\tilde{y}', \mathbf{q})}{q^2}. \quad (5.13)$$

## 5.2 Gravitational Wave Power Spectrum

The spectral density for  $h'$ , when using  $\tilde{y}$  and the dimensionless stree energy correlator  $\tilde{\Pi}$  defined in Eq. 2.24, becomes

$$P_{h'} = [16\pi G (\bar{\epsilon} + \bar{p}) \bar{U}_f^2] L_f^3 \int_{\tilde{y}_s}^{\tilde{y}} d\tilde{y}_1 \int_{\tilde{y}_s}^{\tilde{y}} d\tilde{y}_2 \left( \frac{\partial \tilde{y}}{\partial \tilde{\eta}} \right)^2 \frac{\partial G(\tilde{y}, \tilde{y}_1)}{\partial \tilde{y}} \frac{\partial G(\tilde{y}, \tilde{y}_2)}{\partial \tilde{y}} \times \frac{a_s^8}{a^2(\tilde{y}_1) a^2(\tilde{y}_2)} \frac{\tilde{\Pi}^2(kL_f, k\eta_1, k\eta_2)}{k^2}. \quad (5.14)$$

From the explicit form of the Green's functions derived earlier, we can see  $P_{h'}$  has the correct behavior  $\propto 1/a(\tilde{y})^2$  for the mode deep inside the horizon <sup>9</sup>. The dimensionless source correlator can be obtained from Eq. 2.22, 2.24, 4.49:

$$\tilde{\Pi}^2(kR_{*c}, \beta_c |\eta_1 - \eta_2|) = \frac{\pi}{2} \frac{1}{\bar{U}_f^4} \int d^3 \tilde{q} \mathcal{P}_v(\tilde{q}) \mathcal{P}_v(\tilde{q}) \frac{(1 - \mu^2)^2}{\tilde{q} \tilde{q}^5} \times \cos \left[ c_s \tilde{q} \frac{\beta_c (\eta_1 - \eta_2)}{\beta_c R_{*c}} \right] \cos \left[ c_s \tilde{q} \frac{\beta_c (\eta_1 - \eta_2)}{\beta_c R_{*c}} \right]. \quad (5.15)$$

Here  $\tilde{q} = qR_{*c}$ , a dimensionless quantity, and we use  $L_f = R_{*c}$ . In Fig. 13, we show this autocorrelator of the source as a function of  $\beta_c |\eta_1 - \eta_2|$ . We can see the correlation is quickly lost as  $\beta_c |\eta_1 - \eta_2|$  becomes larger than  $\mathcal{O}(1)$ . Since the source correlator depends only on  $\eta_1 - \eta_2$ , we can change the integration variables from  $\tilde{y}_{1,2}$  to a quantity proportional to  $(\eta_1 - \eta_2)$  and another independent linear combination. For RD and MD, the relation between  $(\eta_1 - \eta_2)$  and  $y_{1,2}$  is given from Eq. 5.5, 5.8:

$$\frac{\beta_c (\eta_1 - \eta_2)}{\beta_c R_{*c}} = \frac{1}{R_{*c} a_s H_s} \begin{cases} y_1 - y_2 \\ 2(\sqrt{y_1} - \sqrt{y_2}) \end{cases}, \quad (5.16)$$

where the upper row applies to RD and lower one to MD. Then for RD, we can make the following change of variables:

$$\begin{cases} y_1 \\ y_2 \end{cases} \Rightarrow \begin{cases} y_1 - y_2 \equiv y_- \\ \frac{y_1 + y_2}{2} \equiv y_+ \end{cases}. \quad (5.17)$$

<sup>8</sup> Alternatively, one can express above Green's functions using the conformal time. The corresponding Green's functions are defined to be zero for  $\eta \leq \eta_0$  and for  $\eta > \eta_0$ .

$$G(\tilde{\eta}, \tilde{\eta}_0) = \begin{cases} \frac{\tilde{\eta}_0}{\tilde{\eta}} \sin(\tilde{\eta} - \tilde{\eta}_0), & \text{RD} \\ \frac{\tilde{\eta}_0}{\tilde{\eta}^3} [(\tilde{\eta}_0 - \tilde{\eta}) \cos(\tilde{\eta} - \tilde{\eta}_0) + (\tilde{\eta}_0 \tilde{\eta} + 1) \sin(\tilde{\eta} - \tilde{\eta}_0)], & \text{MD} \end{cases} \quad (5.11)$$

We note that there is a mistake in the Green's function for the matter dominated universe given in Ref. [67], where instead of  $(\tilde{\eta}_0 - \tilde{\eta}) \cos(\tilde{\eta} - \tilde{\eta}_0)$ , they have  $-(\tilde{\eta}_0 - \tilde{\eta}) \cos(\tilde{\eta} - \tilde{\eta}_0)$ .

<sup>9</sup> For modes deep inside the horizon,  $\tilde{y} \gg 1$  and  $\tilde{y}_0 \gg 1$ . Then both Green's functions take a universal form  $\frac{a_0}{a} \sin(\tilde{\eta} - \tilde{\eta}_0)$ . This implies that  $h' \propto 1/a$ ,  $P_{h'} \propto 1/a^2$  and  $\mathcal{P}_{\text{GW}} \propto 1/a^4$ , behaving like radiation which is true for massless gravitons.

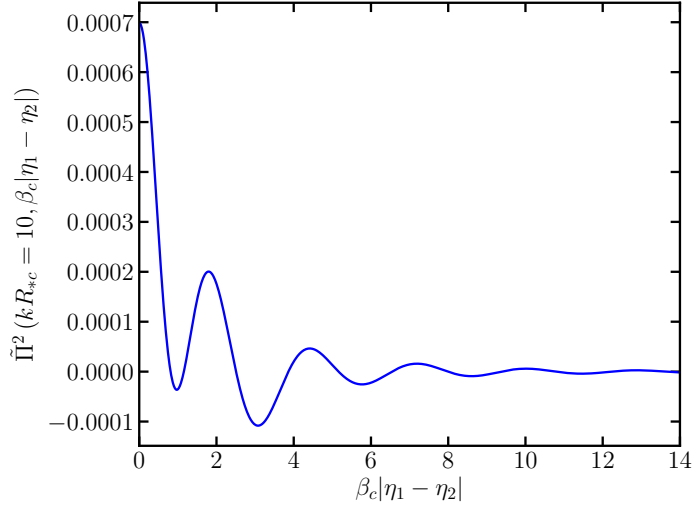


**Figure 13.** Autocorrelation of the source for  $kR_{*c} = 10$ , as shown in explicitly in Eq. 5.15.

The integration range is  $1 - \frac{1}{2}y_- \leq y_+ \leq y_+ + \frac{1}{2}y_-$  when  $1 - y \leq y_- \leq 0$ , and  $1 + \frac{1}{2}y_- \leq y_+ \leq y - \frac{1}{2}y_-$  when  $0 \leq y_- \leq y - 1$ . Similarly for MD, we can perform the following transformations:

$$\begin{cases} y_1 \\ y_2 \end{cases} \Rightarrow \begin{cases} \lambda_1 - \lambda_2 \equiv y_- , \\ \frac{\lambda_1 + \lambda_2}{2} \equiv y_+ . \end{cases} \quad (5.18)$$

where  $\lambda_i = 2\sqrt{y_i}$  and the Jacobian is  $\sqrt{y_1 y_2}$ . The range of integration is  $2 + \frac{1}{2}y_- \leq y_+ \leq 2\sqrt{y} - \frac{1}{2}y_-$  when  $0 \leq y_- \leq 2(\sqrt{y} - 1)$  and  $2 - \frac{1}{2}y_- \leq y_+ \leq 2\sqrt{y} + \frac{1}{2}y_-$  when  $2(1 - \sqrt{y}) \leq y_- \leq 0$ .

It turns out the relation  $y_- \ll y_+$  generally holds, barring special parameter space. This can be seen from Eq. 5.16 by noting that  $\beta_c R_{*c} = (8\pi)^{1/3} v_w \approx 3v_w < 3$ ,  $R_{*c} a_s H_s \sim \mathcal{O}(10^{-3})$  from Fig. 7, and thus  $y_- \sim \mathcal{O}(10^{-3})/v_w \times \beta_c(\eta_1 - \eta_2)$ . Except for extremely small  $v_w$ , which gives highly suppressed gravitational waves, we have  $y_- \ll 1$ . On the contrary,  $y_+ \sim \mathcal{O}(1)$ . Then we have  $y_- \ll y_+$ . This means in the integration over  $y_+$ , we can keep the leading order in  $y_-$ .

Now lets look in more detail at the integrand. For RD and MD, the factor containing Green's function can be written as

$$\frac{\partial G(\tilde{y}, \tilde{y}_1)}{\partial \tilde{y}} \frac{\partial G(\tilde{y}, \tilde{y}_2)}{\partial \tilde{y}} = \begin{cases} \frac{1}{\tilde{y}^2} [c_0^R \tilde{y}^0 + c_{-1}^R \frac{1}{\tilde{y}} + \dots] \\ \frac{1}{\tilde{y}^3} [c_0^M \tilde{y}^0 + c_{-1}^M \frac{1}{\tilde{y}} + \dots] \end{cases} \equiv \begin{cases} \frac{1}{\tilde{y}^2} \\ \frac{1}{\tilde{y}^3} \end{cases} \times \mathcal{G}_2(\tilde{y}, \tilde{y}_1, \tilde{y}_2). \quad (5.19)$$

Then

$$\begin{aligned} \mathcal{P}_{\text{GW}}(y, kR_{*c}) &= \frac{[16\pi G (\bar{\epsilon} + \bar{p}) \bar{U}_f^2]^2}{24\pi^2 H^2 H_s^2} \frac{1}{y^4} (kR_{*c})^3 \\ &\times \int dy_- \tilde{\Pi}^2(kR_{*c}, \beta_c|\eta_1 - \eta_2) \left[ \int dy_+ \frac{\mathcal{G}_2(\tilde{y}, \tilde{y}_1, \tilde{y}_2)}{\tilde{k}^2} \left\{ \frac{y_1^{-2} y_2^{-2}}{y_1^{-3/2} y_2^{-3/2}} \right\} \right]. \end{aligned} \quad (5.20)$$

In the square bracket,  $y_{1,2}$  are understood to be functions of  $y_{\pm}$  (note that  $\tilde{y}$  is defined differently for matter and radiation cases). The reason we associate a factor of  $\tilde{k}^{-2}$  with  $\mathcal{G}_2$  is that  $\mathcal{G}_2 \propto \tilde{k}^2$  to a good approximation. For both RD and MD, the integral over  $y_+$  leads to a result in the following form:

$$\left[ \int dy_+ \dots \right] = \frac{1}{2} \Upsilon(y) \cos(\tilde{k} y_-). \quad (5.21)$$

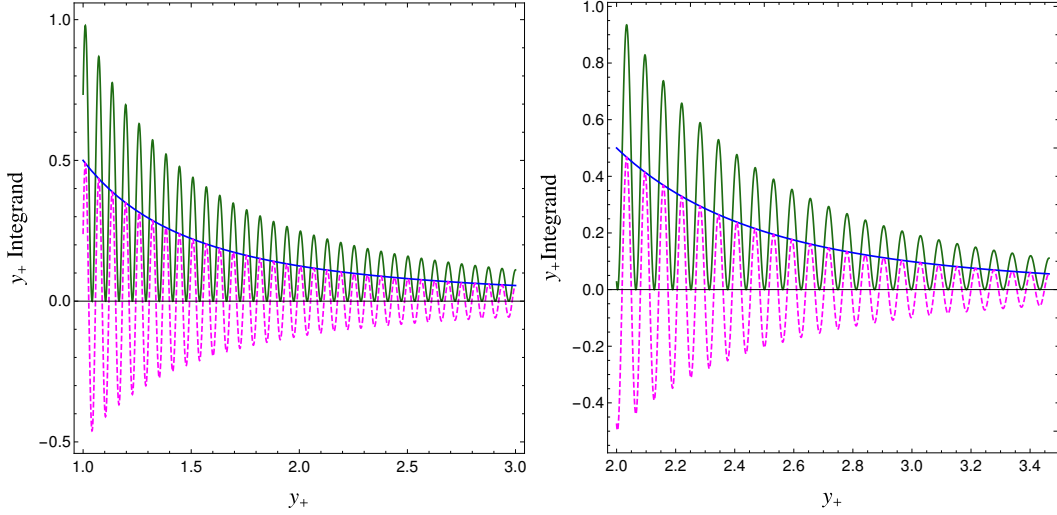


**Figure 14.** The integrand of  $y_+$  integration, with  $y = 3$ . Left is RD and right is MD. The blue is the dominant non-oscillatory part, the magenta dashed is the oscillatory part ( $kR_{*c}$  chosen to be 0.04) and the dark green is the total contribution.

The profile in a wide range of  $y$  is shown in Fig. 15. We can see  $\Upsilon$  of RD is slightly larger than MD. For both cases,  $\Upsilon$  approaches an asymptotic value: 1 for RD and  $2/3$  for MD, irrespective of how long the source lasts. This is due to the dilution of the source over time, which makes the contribution from later time increasingly suppressed. To have a better understanding of the behavior of  $\Upsilon(y)$ , let's see how they can be obtained in a simpler analytical way.

First for RD, neglecting terms suppressed by  $(R_{*c}a_s H_s)$  or  $y^{-1}$ , the dominant contributions to the integrand of the power spectrum are

$$\mathcal{G}_2^{\text{RD}} = \frac{1}{2y_+^2} \left\{ \cos \left[ \tilde{k}y_- \right] + \cos \left[ 2\tilde{k}(y - y_+) \right] \right\} + \dots \quad (5.22)$$

The second term is  $y_-$  independent and is a highly oscillatory function of  $y_+$ , which averages to zero during the integration over  $y_+$ . On the other hand, the first term, a function of  $y_-$ , when integrated, gives the dominant contribution:

$$\Upsilon_{\text{RD}} = 1 - \frac{1}{y}. \quad (5.23)$$

For  $y \gg 1$ , it approaches an asymptotic value of 1. Since this asymptotic value can only be reached for a long enough source, a true phase transition might not satisfy this. We will come to this point later.

Similarly for MD, we can perform analogous manipulations and keep only the leading order and also non-oscillatory term:

$$\mathcal{G}_2^{\text{MD}} = \frac{8}{y_+^4} \cos \left[ \tilde{k}y_- \right] + \dots \quad (5.24)$$

Upon integration, it gives the dominant contribution:

$$\Upsilon_{\text{MD}} = \frac{2}{3} \left( 1 - \frac{1}{y^{3/2}} \right). \quad (5.25)$$

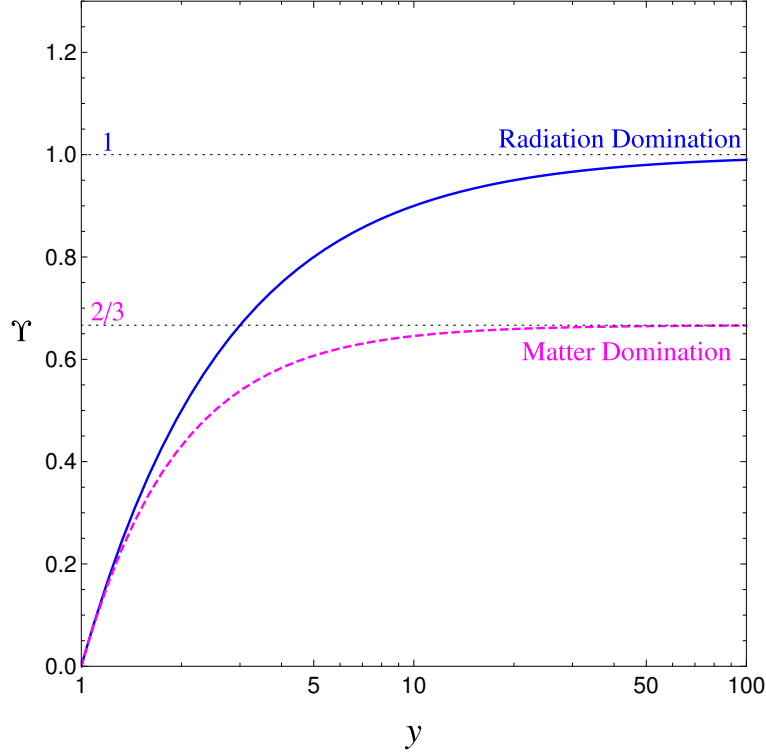


**Figure 15.** The function  $\Upsilon$  for radiation domination(blue solid) and matter domination(magenta dashed).

For  $y \gg 1$ , it approaches the previously observed asymptotic value of  $2/3$ . Thus barring other differences for RD and MD, the different expansion behaviors lead to a suppression of gravitational wave spectrum for MD, when compared with RD.

With  $\Upsilon(y)$  obtained, the power spectrum as a function of  $y$  can be written in the following form

$$\mathcal{P}_{\text{GW}}(y, kR_{*c}) = \frac{[16\pi G (\bar{\epsilon} + \bar{p}) \bar{U}_f^2]^2}{48\pi^2 H^2 H_s^2} \frac{1}{y^4} (kR_{*c})^3 \times \left[ \int dy_- \cos(\tilde{k}y_-) \tilde{\Pi}^2(kR_{*c}, \beta_c |\eta_1 - \eta_2|) \right] \times \Upsilon(y). \quad (5.26)$$

Here note that using Eq. 5.16, we have  $\tilde{k}y_- = k(\eta_1 - \eta_2)$ . The integral over  $y_-$  is obtained by plugging the explicit expression of  $\tilde{\Pi}$ , which results in a three-fold integral. The integration of  $y_-$  over the three trigonometric functions result in a  $\delta$  function, and makes the angle integration of  $\tilde{q}$  in Eq. 5.15 trivial. We are left eventually with a one fold integral over the magnitude of  $\tilde{q}$ , and the spectrum can be put in the following standard form:

$$\mathcal{P}_{\text{GW}}(y, kR_{*c}) = 3\Gamma^2 \bar{U}_f^4 \frac{H_{R,s}^4}{H^2 H_s} (a_s R_{*c}) \frac{(kR_{*c})^3}{2\pi^2} \tilde{P}_{\text{gw}}(kR_*) \times \frac{1}{y^4} \Upsilon(y). \quad (5.27)$$

where  $\Gamma = \bar{w}/\bar{\epsilon} \approx 4/3$ ,  $H_{R,s}$  is defined to contain only the radiation energy density at  $t_s$ :  $H_{R,s} = H_s \sqrt{1 - \kappa_M}$ , and the integral is hidden inside  $\tilde{P}_{\text{gw}}(kR_*)$ :

$$\tilde{P}_{\text{GW}}(kR_*) = \frac{1}{4\pi c_s kR_*} \left( \frac{1 - c_s^2}{c_s^2} \right)^2 \int_{z_-}^{z_+} \frac{dz}{z} \frac{(z - z_+)^2 (z - z_-)^2}{z_+ + z_- - z} \bar{P}_v(z) \bar{P}_v(z_+ + z_- - z). \quad (5.28)$$

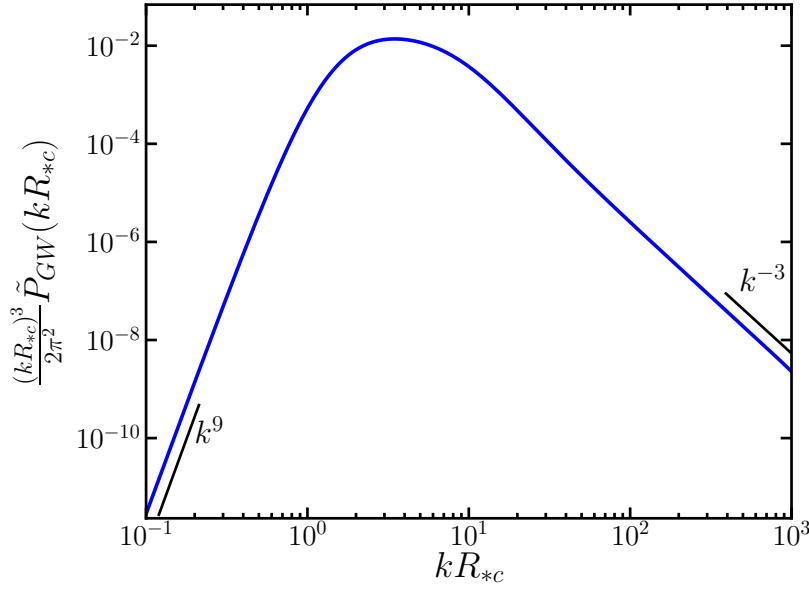


**Figure 16.** The dimensionless gravitational wave power spectrum computed in the sound shell model when  $a = a_* = 1$ . The calculation was performed for a weak phase transition with  $\alpha = 0.0046$ ,  $v_w = 0.92$ , and exponential bubble nucleation. The lifetime of the source is  $\tau_\nu$  and the characteristic length scale is interpreted as the bubble radius. The low and high frequency regimes follow the  $k^9$  and  $k^{-1}$  power law fits respectively (black solid lines)

Here  $z = qR_{*c}$ ,  $z_\pm = \frac{1}{2} \frac{kR_{*c}}{c_s} (1 \pm c_s)$  and  $\bar{P}_v(z) = \frac{\pi^2}{\bar{U}_f^2} \frac{P_v(z)}{z^3}$ . Using Eq. 4.50, the explicit expression for  $\bar{P}_v$  is

$$\bar{P}_v(z) = \frac{1}{64\pi^2 v_w^6} \frac{1}{\bar{U}_f^2} \int d\tilde{T} \tilde{T}^6 \nu(\tilde{T}) \left| A \left( \frac{z\tilde{T}}{(8\pi)^{1/3} v_w} \right) \right|^2. \quad (5.29)$$

Plugging in the explicit expressions of  $H$  and  $H_{R,s}$ , we have

$$\mathcal{P}_{\text{GW}}(y, kR_{*c}) = 3\Gamma^2 \bar{U}_f^4 (H_s a_s R_{*c}) \frac{(kR_{*c})^3}{2\pi^2} \tilde{P}_{\text{gw}}(kR_*) \times \left\{ \frac{1}{\frac{(1-\kappa_M)^2}{\kappa_M y + 1 - \kappa_M}} \right\} \times \Upsilon(y). \quad (5.30)$$

For both RD and MD, the shape of the spectra are the same to a good approximation, and are the same as that derived in the sound shell model and thus the properties of its shape [43] apply here for both cases. In particular, the peak frequency of the spectrum is located at around  $kR_{*c} \approx 10$ . This mean a larger or smaller  $R_*$  can red or blue shift the spectrum respectively. For example, as shown in Fig. 7, increasing  $v_w$  reduces  $R_{*c}$  and thus blue-shift the spectrum. For MD, it has a larger  $R_*$  and thus red-shift the spectrum.

For RD, we recover the result found in Ref. [39], as long as  $\Upsilon(y) = 1$ , which is only true for  $y \gg 1$ . The reason only this asymptotic value is obtained in Ref. [39] is due to the over-simplifying assumptions used (see Appendix B), in which case the second terms in both Eq. 5.23 and 5.25 are missing. Whether or not the asymptotic values can be reached depends on how long the source remains active, and we continue in the next section on this question.

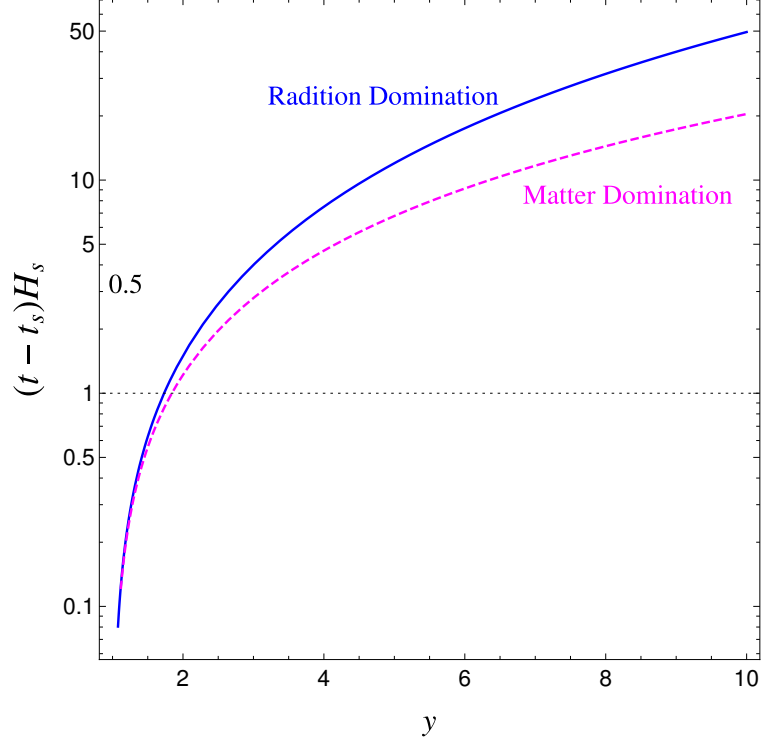


**Figure 17.** Time elapsed since  $t_s$  in unit of Hubble time  $H_s^{-1}$  at  $t_*$ .

### 5.3 Lifetime of the Source

As we saw earlier, the presence of an asymptotic value for  $\Upsilon$  for large  $y$  in both cases is due to the dilution of the source energy density. This asymptotic value was used in Ref. [39] to reach the conclusion that for RD the effective lifetime of the source is a Hubble time  $H_s^{-1}$  for RD, i.e.,  $\tau_v = 1/H_s$ , which as we have seen is only true if  $\Upsilon = 1$  for  $y \gg 1$ . The question is, however, whether this asymptotic value can be reached in a realistic time frame. In Fig. 17, we show the time elapsed since the reference time  $t_s$ , in unit of the Hubble time  $H_s^{-1}$ . For RD,

$$\frac{t - t_s}{1/H_s} = \frac{y^2 - 1}{2}, \quad (5.31)$$

and for MD

$$\frac{t - t_s}{1/H_s} = \frac{2}{3}(y^{3/2} - 1). \quad (5.32)$$

At about a Hubble time,  $\Upsilon \approx 0.2$  for both RD and MD, which is less than a half of the asymptotic value for RD and 60% for MD. We need many Hubble times for  $\Upsilon$  to approach the asymptotic value. The problem is certain physical processes might prohibit the sound waves from being active for such a long time, and thus the asymptotic value might never be reached. One such process is the possible formation of shocks and turbulence. Another is the existence of possible dissipative processes, whose presence damps the sound waves. If either of these processes quenches the sound waves, the asymptotic value will not be achieved. In this case, the effective lifetime is shorter than the Hubble time for RD, and the result obtained with an effective lifetime of a Hubble time overestimates

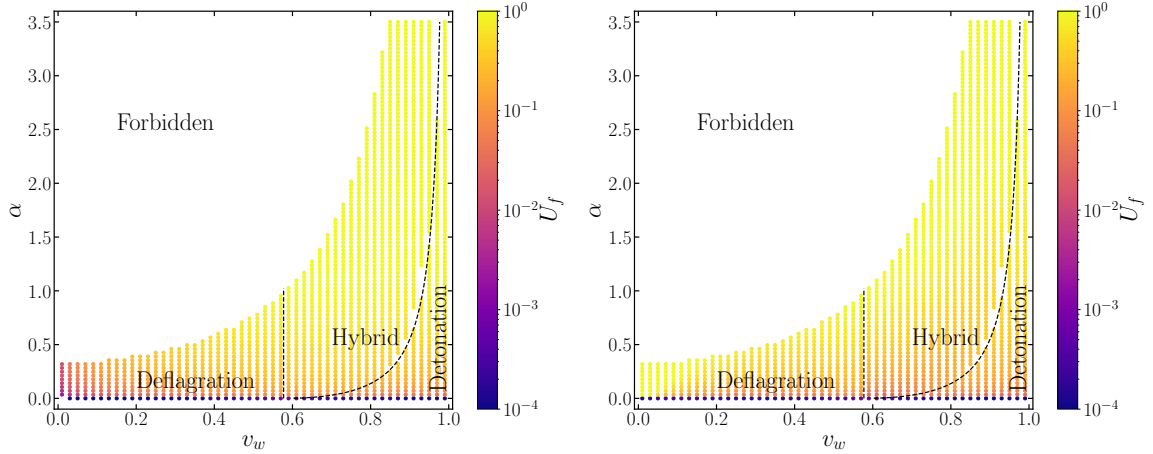


**Figure 18.**  $\bar{U}_f$  on the plane of  $(v_w, \alpha)$ . The left figure is  $\bar{U}_f$  of the fluid around a single bubble. The right figure is  $\bar{U}_f$  of the fluid calculated from the velocity power spectrum.

the gravitational wave production. The time scale for turbulence is roughly [40, 94]

$$\tau_{\text{sh}} \sim \frac{L_f}{\bar{U}_f} \sim \frac{R_*}{\bar{U}_f}. \quad (5.33)$$

Therefore

$$\frac{\tau_{\text{sh}}}{1/H_s} \sim \frac{H_s R_*}{\bar{U}_f}. \quad (5.34)$$

As we have seen in Fig. 7,  $H_s R_s \sim 10^{-3}$  and different expansion histories lead to larger or smaller values. To delay the appearance of turbulence and thus approach the asymptotic value of  $\Upsilon$  thus requires smaller fluid velocity  $\bar{U}_f$  or larger bubble separation. While  $H_s R_*$  depends on specific expansion behavior adopted, the value of  $\bar{U}_f$  is more or less universal, and its value is shown in Fig. 18 on the plane of  $(v_w, \alpha)$  by solving the velocity profile for the entire plane. Therefore whether or not above ratio becomes large enough depends on the details of the phase transition in a given cosmological context. Even in cases where the turbulence is delayed or not present, i.e., for sufficiently strong or weak phase transitions respectively, the damping of the sound waves caused by some weak processes could still shorten the lifetime in the form of shear viscosity [39]. It seem unlikely for any scenario to be very close to the asymptotic value.

#### 5.4 Spectrum Today

We will mainly consider the case of RD as it is the most frequently encountered scenario. Denote the temperature after the gravitational wave production as  $T_e$  with the scale factor being  $a_e$ . The amount of redshifting is described by the scale factor ratio  $a_e/a_0$ . For radiation in thermal equilibrium and in adiabatic expansion, the relation between  $a_e$  and  $a_0$  is governed by entropy conservation:

$$g_s(T_e) a_e^3 T_e^3 = g_s(T_{\gamma 0}) a_0^3 T_{\gamma 0}^3, \quad (5.35)$$

where  $g_s$  is the relativistic degrees of freedom for entropy;  $T_{\gamma 0}$  is the temperature of the CMB photon with  $T_{\gamma 0} \approx 2.73K$ . At the present time, the relativistic species includes photons and decoupled



neutrinos, thus  $g_s = 2 + \frac{7}{8} \times 2N_{\text{eff}}(\frac{4}{11})^{3/3} \approx 3.94$  for  $N_{\text{eff}} = 3.046$ . Using these, the ratio of the scale factor can be put into the following form:

$$\frac{a_e}{a_0} = 1.65 \times 10^{-5} \left( \frac{g_s(T_e)}{100} \right)^{1/6} \left( \frac{T_e}{100\text{GeV}} \right) \left( \frac{1\text{Hz}}{H_e} \right). \quad (5.36)$$

For the peak frequency, its precise value is not fully settled. For the peak at  $kR_* = z_p$ <sup>10</sup> where  $z_p \approx 10$  [40], the frequency at  $t_e$  is

$$f_p = \frac{z_p}{2\pi R_*(t_e)}, \quad (5.37)$$

where  $R_*(t_e)$  is evaluated at the end of the gravitational wave production and note all previously generated gravitational waves at higher frequencies at  $kR_{*c} = z_p$  have all redshifted to the frequency produced at  $t_e$ . Then the corresponding frequency today is

$$f_{\text{SW}} = 2.65 \times 10^{-5} \text{Hz} \left( \frac{g_s(T_e)}{100} \right)^{1/6} \left( \frac{T_e}{100\text{GeV}} \right) \left( \frac{z_p}{10} \right) \left( \frac{1}{H_e R_*(t_e)} \right). \quad (5.38)$$

We can express  $R_*$  by  $\beta(v_w)$  using Eq. 3.50, so that,

$$\frac{1}{H_e R_*(t_e)} = (8\pi)^{-1/3} \frac{a(t_f)}{a(t_e)} \frac{1}{v_w} \frac{\beta(v_w)}{H_e} = (8\pi)^{-1/3} \frac{1}{v_w} \frac{\beta(v_w)}{H_e} \times \frac{1}{y}. \quad (5.39)$$

Here we neglect the very small difference between  $t_f$ , the time when all the bubbles have disappeared and  $t_s$ , and we have shown explicitly the dependence of  $\beta$  on  $v_w$ . Also note  $\beta$  is evaluated at  $t_f$  when  $I(t_f) = 1$ . The factor  $y^{-1}$  is significant when the lifetime of the source is long. Then the present peak frequency becomes

$$f_{\text{SW}} = 8.97 \times 10^{-6} \text{Hz} \frac{1}{v_w} \left( \frac{g_s(T_e)}{100} \right)^{1/6} \left( \frac{T_e}{100\text{GeV}} \right) \left( \frac{z_p}{10} \right) \left[ \frac{\beta(v_w)/y}{H_e} \right]. \quad (5.40)$$

For the energy fraction of gravitational waves, the dilution of gravitational waves leads to the following connection:

$$\begin{aligned} h^2 \Omega_{\text{GW}}(t_0, f) &= h^2 \left( \frac{a_e}{a_0} \right)^4 \left( \frac{H_e}{H_0} \right)^2 \Omega_{\text{GW}}(t_e, a_0 f / a_e), \\ &= 1.66 \times 10^{-5} \left( \frac{100}{g_s(T_e)} \right)^{1/3} \Omega_{\text{GW}}(t_e, a_0 f / a_e). \end{aligned} \quad (5.41)$$

Here  $h \approx 0.673$ , the Hubble parameter today in unit of 100km/s/Mpc. Then plugging the explicit expression for  $\mathcal{P}_{\text{GW}}$  in Eq. 5.30, we have

$$h^2 \Omega_{\text{GW}}(f) = 4.98 \times 10^{-5} \left( \frac{100}{g_s(T_e)} \right)^{1/3} \Gamma^2 \bar{U}_f^4 [H_s R_*(t_s)] A \mathcal{S}_{\text{SW}}(f) \Upsilon(y). \quad (5.42)$$

Here we have defined  $A \mathcal{S}_{\text{SW}}(f)$  to be  $(kR_*)^3 \tilde{P}_{\text{gw}}(kR_*) / (2\pi^2)$  with appropriate redshifting factors included. One can either use the prediction from the sound shell model to determine  $A \mathcal{S}_{\text{SW}}(f)$ , or

<sup>10</sup> We use a notation where  $k$  in  $kR_*$  is physical wavenumber, and  $k$  in  $kR_{*c}$  is a comoving wavenumber.

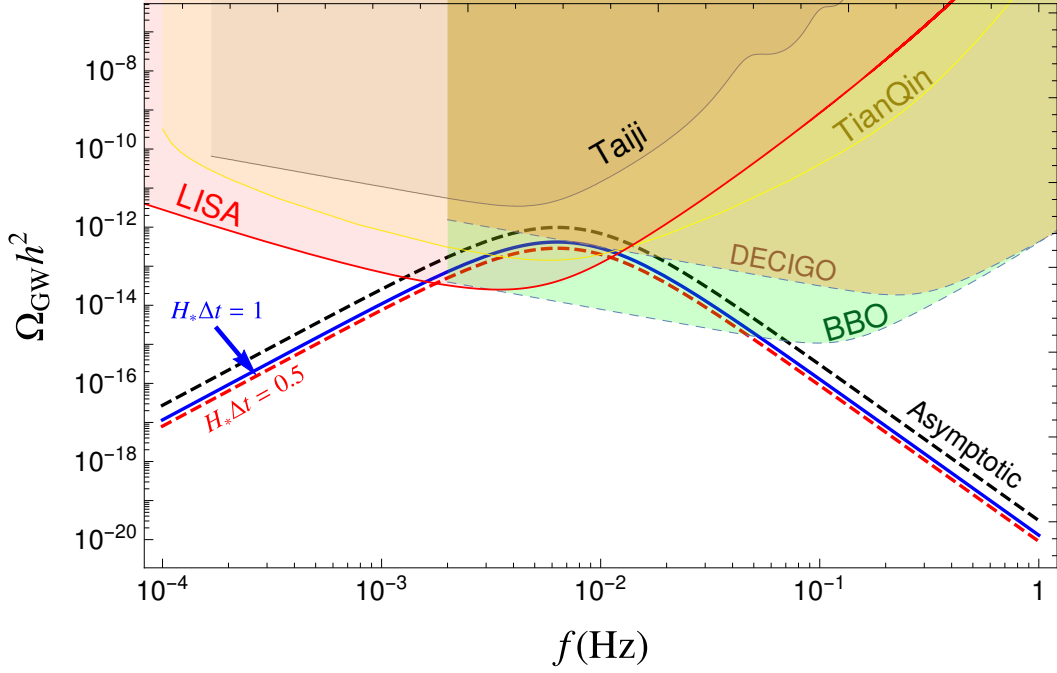


**Figure 19.** The present day gravitational wave energy density spectra for  $H_* \Delta t = 0.5, 1$  and for  $H_* \Delta t \gg 1$  when it takes the asymptotic form. Here  $\Delta t = t - t_s$  and is the time elapsed since  $t_s$ , the time when the source becomes active. In all three cases,  $v_w = 0.3$ ,  $\alpha = 0.1$ ,  $T_e = 100\text{GeV}$  and  $\beta/(yH_*) = 100$ . The shaded regions at the top are experimental sensitive regions for several proposed space-based detectors.

use result from numerical simulations [40]. We choose the latter as it should give a more accurate result, in which case  $A \approx 0.058$  and [2]

$$\mathcal{S}_{\text{sw}}(f) = \left( \frac{f}{f_{\text{sw}}} \right)^3 \left[ \frac{7}{4 + 3(f/f_{\text{sw}})^2} \right]^{7/2}. \quad (5.43)$$

For the term  $H_s R_*(t_s)$ , similar to Eq. 5.39, we can write

$$H_s R_*(t_s) = (8\pi)^{1/3} v_w \frac{H_s}{\beta(v_w)}. \quad (5.44)$$

Therefore the final spectrum is

$$h^2 \Omega_{\text{GW}}(f) = 8.5 \times 10^{-6} \left( \frac{100}{g_s(T_e)} \right)^{1/3} \Gamma^2 \bar{U}_f^4 \left[ \frac{H_s}{\beta(v_w)} \right] v_w \mathcal{S}_{\text{sw}}(f) \times \Upsilon(y). \quad (5.45)$$

For a long lifetime of the source, the main changes are the suppression factor  $\Upsilon(y)$ . In Fig. 19, we show the spectra for several choices of  $H_* \Delta t$ , with  $z_p = 10$  (see caption for more details).

For MD, apparently the extra dominant matter content will decay to radiation at some time later, which will inject entropy to the standard radiation sector. This can be studied using two methods. In the first method, one can assume a very quick and thus instantaneous decay of the matter, which then allows to use energy conservation to get the new heated radiation temperature. In the second method, a more precise account of the matter decay is provided, with the conclusion that there is no heating up of the radiation but one gets a slower cooling of the radiation, as was firstly pointed out in

Ref. [81]. Therefore one needs to follow more closely the entropy evolution by taking into account finite matter decay width, following the procedure of Ref. [81] or a more closely related example studied in Ref. [68]. This however introduces extra model dependent varieties and is beyond the scope of this work.

## 6 Summary

We studied in detail the cosmological first order phase transition and the calculation of resulting stochastic gravitational waves in an expanding universe, with radiation and matter dominated universe as two representative examples. Firstly we studied the changes to process of bubble formation and collision, including important observables such as the mean bubble separation and its relation with  $\beta$ . We also derived the unbroken bubble wall area, the bubble conformal lifetime distribution which are needed for the calculation of the gravitational wave spectrum. We then derived the full set of differential equations as used in numerical simulations in an expanding universe. We found that simple rescalings works such that the equations governing the velocity profile around a single bubble maintains the same form as in Minkowski spacetime and that the velocity profile remains the same when appropriate substitution of variables are used. We then used and generalized the sound shell model to the expanding universe and derived the velocity power spectrum. This result is used to derive analytically the gravitational wave power spectrum from the sound waves, the dominant source. We found that the standard formula of the spectrum needs to include an additional suppression factor  $\Upsilon$ , which is a function of the lifetime of the source. For radiation domination, the asymptotic value of  $\Upsilon$  is 1 when the lifetime of the source is very long, and corresponds to the usually adopted spectrum in the literature. This asymptotic value however can not be reached as the onset of shocks and turbulence may disrupt the sound waves and possible dissipative processes may further damp it. Therefore an additional suppression factor needs to be taken into account when using the gravitational wave spectrum from sound waves and we provided simple analytical expression for  $\Upsilon$ .

## 7 Acknowledgments

HG and KS are supported by DOE Grant desc0009956. TRIUMF receives federal funding via a contribution agreement with the National Research Council of Canada. We thank Mark Hindmarsh for helpful communications. We acknowledge Elizabeth Loggia for her early involvement in this project. May our field become more accommodating to mothers.

## A The Example Effective Potential

Here we provide details of the example effective potential used in Sec. 3, so that those results can be reproduced more easily. The effective potential was originally used as a high temperature approximation for the standard model, given by

$$V(\phi, T) = D(T^2 - T_0^2)\phi^2 - ET\phi^3 + \frac{\lambda}{4}\phi^4. \quad (\text{A.1})$$

Here  $D > 0$ ,  $E > 0$ ,  $\lambda > 0$  and  $\lambda$  has a weak dependence on  $T$ . The first term has a positive coefficient when  $T > T_0$  to restore the symmetry. The third, the cubic term, when is sufficiently smaller, helps create a barrier together with the first term, and creates another minimum. Since this example is only used to provide a simple benchmark effective potential to show the effects of

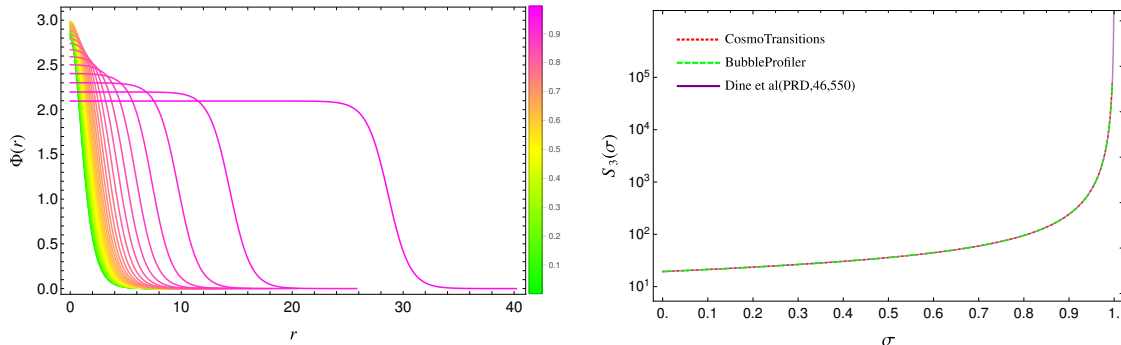


**Figure 20.** Left panel: the bounce solutions for the example effective potential with rescaled fields and coordinates used in this work for different choices of  $\alpha$ , with the colormap denoting values of  $\alpha$ . Right panel: comparison of the corresponding  $S_3(T)/T$  obtained with CosmoTransitions and the analytical fit provided in Ref. [95].

the expansion of the universe, we will take these parameters to be  $T$  independent. It should be noted that an effective potential of this form can characterize features of a wide class of beyond the standard model scenarios in the high temperature approximation. We will use this effective potential to calculate bounce solutions and corresponding parameters relevant for the phase transition.

Though there are four free parameters for this simple effective potential, a rescaling of both the coordinates and the scalar fields allows to reduce to only one dynamical parameter [95]. The rescaled fields and coordinates are defined as  $\Phi = 2ET\phi/M^2$  and  $X = Mx$ . The Lagrangian then becomes

$$\mathcal{L} = \frac{M^6}{4E^2T^2} \left[ \frac{1}{2}(\partial_X \Phi)^2 - \frac{1}{2}\Phi^2 + \frac{1}{2}\Phi^3 - \frac{1}{8}\sigma\Phi^4 \right], \quad (\text{A.2})$$

where  $\sigma \equiv \lambda M^2/(2E^2T^2)$ . The behavior of the effective potential for the rescaled fields during the phase transition is solely controlled by  $\sigma$ . When  $\sigma < 9/8$ , a second minimum develops. The corresponding temperature is:

$$T = \sqrt{\frac{T_0^2}{1 - \frac{9E^2}{8\lambda D}}}. \quad (\text{A.3})$$

When  $\sigma = 1$ , this minimum is degenerate with the one at the origin, which corresponds to a critical temperature of

$$T_c = \sqrt{\frac{T_0^2}{1 - \frac{E^2}{\lambda D}}}. \quad (\text{A.4})$$

Therefore for the rescaled field  $\Phi$  and coordinate  $X$ , there is essentially one parameter  $\sigma$  that determines the shape of the potential. Calculating the bounce solution and  $S_3$  for all choices of  $\sigma$  is sufficient to cover the full four parameter space. Define the  $S_3$  action for the rescaled fields and coordinates as  $\tilde{S}_3(\sigma)$ , then the  $S_3(T)$  for the original four parameter theory can be obtained directly as

$$\frac{S_3(T)}{T} = \frac{M^3}{4E^2T^3} \tilde{S}_3(\sigma). \quad (\text{A.5})$$

The bounce solutions for various choices of  $\alpha$  are shown in the left panel of Fig. A and the corresponding  $S_3(\sigma)$  shown as red dotted and green dashed lines for solutions solved from CosmoTransitions [96] and BubbleProfiler [97] respectively. In this plot, there is also a purple curve, corresponding to the analytical fit in Ref. [95]:

$$\tilde{S}_3(\sigma) = 4 \times 4.85 \times \left\{ 1 + \frac{\sigma}{4} \left[ 1 + \frac{2.4}{1-\sigma} + \frac{0.26}{(1-\sigma)^2} \right] \right\}. \quad (\text{A.6})$$

We can see in the all the region plotted, the three results agree very well with each other. So our results in previous sections can be followed by simply choosing above analytical fit. For the example used in Sec. 3,  $T_0 = 75\text{GeV}$ ,  $E = D = 0.1$  and  $\lambda = 0.2$ , which gives  $T_c = 106.066\text{GeV}$ .

## B The Previously Derived Effective Lifetime of the Source

Here we revisit the deviation that led to the conclusion that the effective lifetime of the source is one Hubble time in a radiation dominated universe, as was originally obtained in Ref. [39]. We will follow closely their notations, using the conformal time  $\eta$  as variable instead of  $y$ , and using  $a_*$  rather than  $a_s$ . Also we study both RD and MD, though only RD is studied in Ref. [39].

We start with Eq. 2.14 and do the integrals over  $\tilde{\eta}_1$  and  $\tilde{\eta}_2$ . We can keep only the leading contribution by neglecting the highly oscillatory part in the Green's functions. This means for the trigonometric function, we keep only the parts with argument  $(\tilde{\eta}_1 - \tilde{\eta}_2)$  and find

$$\begin{aligned} & \frac{\partial G(\tilde{\eta}, \tilde{\eta}_1)}{\partial \tilde{\eta}} \frac{\partial G(\tilde{\eta}, \tilde{\eta}_2)}{\partial \tilde{\eta}} \\ &= \frac{\tilde{\eta}_1 \tilde{\eta}_2}{2} \times \left\{ \begin{array}{l} \tilde{\eta}^{-2}(1 + \tilde{\eta}^{-2}) \cos(\tilde{\eta}_1 - \tilde{\eta}_2), \\ \tilde{\eta}^{-4}(1 + 3\tilde{\eta}^{-2} + 9\tilde{\eta}^{-4}) [(\tilde{\eta}_1 - \tilde{\eta}_2) \sin(\tilde{\eta}_1 - \tilde{\eta}_2) + (1 + \tilde{\eta}_1 \tilde{\eta}_2) \cos(\tilde{\eta}_1 - \tilde{\eta}_2)], \end{array} \right. \quad (\text{B.1}) \end{aligned}$$

where the upper and lower row applies to radiation and matter dominated universe respectively. Now switch integration variables from  $\tilde{\eta}_1$  and  $\tilde{\eta}_2$  to  $x \equiv (\tilde{\eta}_1 + \tilde{\eta}_2)/2$  and  $z = \tilde{\eta}_1 - \tilde{\eta}_2$ . This results in the relation  $\tilde{\eta}_1 \tilde{\eta}_2 = x^2 - \frac{z^2}{4}$ . Under these manipulations, the power spectral density of  $h'$  becomes:

$$\begin{aligned} P_{h'} &= [16\pi G (\bar{\epsilon} + \bar{p}) \bar{U}_f^2]^2 L_f^3 \left\{ \frac{\tilde{\eta}^{-2}(1 + \tilde{\eta}^{-2})}{\tilde{\eta}^{-4}(1 + 3\tilde{\eta}^{-2} + 9\tilde{\eta}^{-4})} \right\} \int dx \int dz \frac{1}{k^2} \frac{\tilde{\eta}_1 \tilde{\eta}_2 a_*^8}{a^2(\eta_1) a^2(\eta_2)} \\ &\quad \times \frac{1}{2} \left\{ \begin{array}{l} \cos z \\ z \sin z + (1 + x^2 - \frac{z^2}{4}) \cos z \end{array} \right\} \tilde{\Pi}^2(\tilde{L}_f, \tilde{\eta}_1, \tilde{\eta}_2). \quad (\text{B.2}) \end{aligned}$$

Here  $\tilde{L}_f \equiv kL_f$ . The expression can be reorganized to show the correct dependence on  $a(\eta)$  and we have for the correlator of  $h$ :

$$\begin{aligned} P_h &= \frac{a_*^6}{a^4(\eta)} \frac{1}{k^2} [16\pi G (\bar{\epsilon} + \bar{p}) \bar{U}_f^2]^2 L_f^3 \left\{ \frac{1 + \tilde{\eta}^{-2}}{1 + 3\tilde{\eta}^{-2} + 9\tilde{\eta}^{-4}} \right\} \int_{\tilde{\eta}_*}^{\tilde{\eta}} dx \int dz \\ &\quad \times \frac{1}{2} \left\{ \begin{array}{l} \frac{\tilde{\eta}_*^2}{x^2 - z^2/4} \\ \frac{\tilde{\eta}_*^4}{(x^2 - z^2/4)^3} \end{array} \right\} \left\{ \begin{array}{l} \cos z \\ z \sin z + (1 + x^2 - \frac{z^2}{4}) \cos z \end{array} \right\} \tilde{\Pi}^2(\tilde{L}_f, \tilde{\eta}_1, \tilde{\eta}_2). \quad (\text{B.3}) \end{aligned}$$

As we have seen the source is largely stationary, that is, the correlator  $\tilde{\Pi}^2(\tilde{L}_f, \tilde{\eta}_1, \tilde{\eta}_2)$  depends only on  $z$  but not on  $x$ . Then it can be written as  $\tilde{\Pi}^2(\tilde{L}_f, z)$ . Also the autocorrelation time  $z$  is very small compared with the Hubble time, so we can neglect the  $z$  dependence on the denominators in the first

curly bracket and keep only the  $x^2$  term for MD in the second curly bracket, which then allows the integration over  $x$ , giving

$$\int_{\tilde{\eta}_*}^{\tilde{\eta}} dx \frac{1}{x^2} = \frac{1}{\tilde{\eta}_*} - \frac{1}{\tilde{\eta}}, \quad \int_{\tilde{\eta}_*}^{\tilde{\eta}} dx \frac{1}{x^4} = \frac{1}{3} \left( \frac{1}{\tilde{\eta}_*^3} - \frac{1}{\tilde{\eta}^3} \right). \quad (\text{B.4})$$

Here is where things go wrong. The second term for RD is neglected in Ref. [39]. This leads to a result that corresponds to the asymptotic value  $\Upsilon = 1$  for RD, and as we have seen the short duration of the source does not allow to neglect this term. Lets continue to reproduce the result of Ref. [39] by keeping only the first term. This gives

$$\begin{aligned} P_h &= \frac{a_*^6}{a^4(\eta)} \frac{1}{k^2} [16\pi G (\bar{\epsilon} + \bar{p}) \bar{U}_f^2]^2 L_f^3 \left\{ \frac{1 + \tilde{\eta}^{-2}}{(1 + 3\tilde{\eta}^{-2} + 9\tilde{\eta}^{-4})/3} \right\} \tilde{\eta}_* \\ &\quad \times \int dz \frac{\cos(z)}{2} \tilde{\Pi}^2(\tilde{L}_f, z) \\ &= \frac{a_*^4}{a^4(\eta)} [16\pi G (\bar{\epsilon} + \bar{p}) \bar{U}_f^2]^2 L_f^3 \left\{ \frac{1 + \tilde{\eta}^{-2}}{(1 + 3\tilde{\eta}^{-2} + 9\tilde{\eta}^{-4})/3} \right\} (a_* \eta_*) (a_* L_f) \tilde{P}_{\text{GW}}(k L_f). \end{aligned} \quad (\text{B.5})$$

In the second line, the following definition is used:

$$\tilde{P}_{\text{GW}}(k L_f) = \frac{1}{k L_f} \int dz \frac{\cos z}{2} \tilde{\Pi}^2(\tilde{L}_f, z). \quad (\text{B.6})$$

The variables appearing in above equations can further be reorganized so that we have a result similar to Eq.(A10) in Ref. [39]:

$$\begin{aligned} \mathcal{P}_{\text{GW}}(t, k) &= 3\Gamma^2 \bar{U}_f^4 \left( \frac{a_*^4}{a^4} \frac{H_{*R}^4}{H^2 H_*^2} \right) \left\{ \frac{1 + \tilde{\eta}^{-2}}{(1 + 3\tilde{\eta}^{-2} + 9\tilde{\eta}^{-4})/3} \right\} \\ &\quad \times (H_* a_* \eta_*) (H_* a_* L_f) \frac{(k L_f)^3}{2\pi^2} \tilde{\mathcal{P}}_{\text{GW}}(k L_f). \end{aligned} \quad (\text{B.7})$$

For RD,  $H_* a_* \eta_* = 1$  and  $a_* L_f$  is the physical length scale ( $L_f^*$  in Ref. [39]). If we also neglect the variation of the Hubble rate from  $H_*$  to  $H$ , and since in this case  $H_{*R} = H_*$ , and also neglect the terms suppressed by  $1/\tilde{\eta}$  in the curly bracket due to the assumed relation  $\tilde{\eta} \gg \tilde{\eta}_*$ , then the result for RD reduces to Eq.(A11) in Ref. [39]. So the main point is we can not assume  $\tilde{\eta} \gg \tilde{\eta}_*$  and neglect the second term in Eq. B.4. Because  $H_* a_* \eta_* = 1$  and also because the power spectrum in Minkowski spacetime is proportional to  $H_* \tau_{\text{sh}}$ , Ref. [39] concluded that the effective lifetime is a Hubble time. This is true if indeed  $\tilde{\eta} \gg \tilde{\eta}_*$ , but as we have seen it requires many Hubble times for the asymptotic value to be reached. The sound wave, however, is likely to be disrupted by the onset of shocks or turbulence or damped by other dissipative processes, which certainly do not allow the sound wave to remain active that long for the asymptotic value to be reached.

While non-relevant here for MD, we can still compare its asymptotic value with what we already find in previous sections. From above equation we can see the quantity in the curly bracket is  $1/3$  for MD and  $1$  for RD. But for MD,  $H_* a_* \eta_* = 2$ , then the asymptotic value of  $\Upsilon$  is  $2/3$  for MD, which is consistent with our previous result.

## References

- [1] C. Caprini *et al.*, ‘‘Science with the space-based interferometer eLISA. II: Gravitational waves from cosmological phase transitions,’’ *JCAP* **1604** no. 04, (2016) 001, [arXiv:1512.06239](https://arxiv.org/abs/1512.06239) [[astro-ph.CO](https://arxiv.org/abs/1512.06239)].

- [2] D. J. Weir, “Gravitational waves from a first order electroweak phase transition: a brief review,” *Phil. Trans. Roy. Soc. Lond.* **A376** no. 2114, (2018) 20170126, [arXiv:1705.01783 \[hep-ph\]](#).
- [3] A. Mazumdar and G. White, “Cosmic phase transitions: their applications and experimental signatures,” [arXiv:1811.01948 \[hep-ph\]](#).
- [4] G. Bertone *et al.*, “Gravitational wave probes of dark matter: challenges and opportunities,” [arXiv:1907.10610 \[astro-ph.CO\]](#).
- [5] C. Caprini *et al.*, “Detecting gravitational waves from cosmological phase transitions with LISA: an update,” *JCAP* **03** (2020) 024, [arXiv:1910.13125 \[astro-ph.CO\]](#).
- [6] E. Barausse *et al.*, “Prospects for Fundamental Physics with LISA,” [arXiv:2001.09793 \[gr-qc\]](#).
- [7] **LIGO Scientific, Virgo** Collaboration, B. P. Abbott *et al.*, “Upper Limits on the Stochastic Gravitational-Wave Background from Advanced LIGO’s First Observing Run,” *Phys. Rev. Lett.* **118** no. 12, (2017) 121101, [arXiv:1612.02029 \[gr-qc\]](#). [Erratum: *Phys.Rev.Lett.* 119, 029901 (2017)].
- [8] **LIGO Scientific, Virgo** Collaboration, B. Abbott *et al.*, “Search for the isotropic stochastic background using data from Advanced LIGO’s second observing run,” *Phys. Rev. D* **100** no. 6, (2019) 061101, [arXiv:1903.02886 \[gr-qc\]](#).
- [9] C. Grojean and G. Servant, “Gravitational Waves from Phase Transitions at the Electroweak Scale and Beyond,” *Phys. Rev.* **D75** (2007) 043507, [arXiv:hep-ph/0607107 \[hep-ph\]](#).
- [10] V. Vaskonen, “Electroweak baryogenesis and gravitational waves from a real scalar singlet,” *Phys. Rev.* **D95** no. 12, (2017) 123515, [arXiv:1611.02073 \[hep-ph\]](#).
- [11] G. Dorsch, S. Huber, T. Konstandin, and J. No, “A Second Higgs Doublet in the Early Universe: Baryogenesis and Gravitational Waves,” *JCAP* **05** (2017) 052, [arXiv:1611.05874 \[hep-ph\]](#).
- [12] A. Beniwal, M. Lewicki, M. White, and A. G. Williams, “Gravitational waves and electroweak baryogenesis in a global study of the extended scalar singlet model,” [arXiv:1810.02380 \[hep-ph\]](#).
- [13] C. Delaunay, C. Grojean, and J. D. Wells, “Dynamics of Non-renormalizable Electroweak Symmetry Breaking,” *JHEP* **04** (2008) 029, [arXiv:0711.2511 \[hep-ph\]](#).
- [14] M. Chala, C. Krause, and G. Nardini, “Signals of the electroweak phase transition at colliders and gravitational wave observatories,” *JHEP* **07** (2018) 062, [arXiv:1802.02168 \[hep-ph\]](#).
- [15] S. A. Ellis, S. Ipek, and G. White, “Electroweak Baryogenesis from Temperature-Varying Couplings,” *JHEP* **08** (2019) 002, [arXiv:1905.11994 \[hep-ph\]](#).
- [16] A. Alves, D. Gonalves, T. Ghosh, H.-K. Guo, and K. Sinha, “Di-Higgs Production in the  $4b$  Channel and Gravitational Wave Complementarity,” *JHEP* **03** (2020) 053, [arXiv:1909.05268 \[hep-ph\]](#).
- [17] A. Alves, T. Ghosh, H.-K. Guo, K. Sinha, and D. Vagie, “Collider and Gravitational Wave Complementarity in Exploring the Singlet Extension of the Standard Model,” *JHEP* **04** (2019) 052, [arXiv:1812.09333 \[hep-ph\]](#).
- [18] J. Ellis, M. Lewicki, J. M. No, and V. Vaskonen, “Gravitational wave energy budget in strongly supercooled phase transitions,” *JCAP* **06** (2019) 024, [arXiv:1903.09642 \[hep-ph\]](#).
- [19] A. P. Morais and R. Pasechnik, “Probing multi-step electroweak phase transition with multi-peaked primordial gravitational waves spectra,” *JCAP* **04** (2020) 036, [arXiv:1910.00717 \[hep-ph\]](#).
- [20] A. Addazi, A. Marcian, and R. Pasechnik, “Probing Trans-electroweak First Order Phase Transitions from Gravitational Waves,” *MDPI Physics* **1** no. 1, (2019) 92–102, [arXiv:1811.09074 \[hep-ph\]](#).

- [21] C. Wainwright, S. Profumo, and M. J. Ramsey-Musolf, “Gravity Waves from a Cosmological Phase Transition: Gauge Artifacts and Daisy Resummations,” *Phys. Rev. D* **84** (2011) 023521, [arXiv:1104.5487 \[hep-ph\]](#).
- [22] P. Schwaller, “Gravitational Waves from a Dark Phase Transition,” *Phys. Rev. Lett.* **115** no. 18, (2015) 181101, [arXiv:1504.07263 \[hep-ph\]](#).
- [23] J. Jaeckel, V. V. Khoze, and M. Spannowsky, “Hearing the signal of dark sectors with gravitational wave detectors,” *Phys. Rev. D* **94** no. 10, (2016) 103519, [arXiv:1602.03901 \[hep-ph\]](#).
- [24] M. Chala, G. Nardini, and I. Sobolev, “Unified explanation for dark matter and electroweak baryogenesis with direct detection and gravitational wave signatures,” *Phys. Rev. D* **94** no. 5, (2016) 055006, [arXiv:1605.08663 \[hep-ph\]](#).
- [25] A. Addazi, “Limiting First Order Phase Transitions in Dark Gauge Sectors from Gravitational Waves experiments,” *Mod. Phys. Lett. A* **32** no. 08, (2017) 1750049, [arXiv:1607.08057 \[hep-ph\]](#).
- [26] I. Baldes, “Gravitational waves from the asymmetric-dark-matter generating phase transition,” *JCAP* **05** (2017) 028, [arXiv:1702.02117 \[hep-ph\]](#).
- [27] A. Addazi and A. Marciano, “Gravitational waves from dark first order phase transitions and dark photons,” *Chin. Phys. C* **42** no. 2, (2018) 023107, [arXiv:1703.03248 \[hep-ph\]](#).
- [28] D. Croon, V. Sanz, and G. White, “Model Discrimination in Gravitational Wave spectra from Dark Phase Transitions,” *JHEP* **08** (2018) 203, [arXiv:1806.02332 \[hep-ph\]](#).
- [29] I. Baldes and C. Garcia-Cely, “Strong gravitational radiation from a simple dark matter model,” *JHEP* **05** (2019) 190, [arXiv:1809.01198 \[hep-ph\]](#).
- [30] M. Fairbairn, E. Hardy, and A. Wickens, “Hearing without seeing: gravitational waves from hot and cold hidden sectors,” *JHEP* **07** (2019) 044, [arXiv:1901.11038 \[hep-ph\]](#).
- [31] D. Dunsy, L. J. Hall, and K. Harigaya, “Dark Matter, Dark Radiation and Gravitational Waves from Mirror Higgs Parity,” *JHEP* **02** (2020) 078, [arXiv:1908.02756 \[hep-ph\]](#).
- [32] P. Archer-Smith, D. Linthorne, and D. Stolarski, “Gravitational Wave Signals from Multiple Hidden Sectors,” *Phys. Rev. D* **101** no. 9, (2020) 095016, [arXiv:1910.02083 \[hep-ph\]](#).
- [33] E. Hall, T. Konstandin, R. McGehee, and H. Murayama, “Asymmetric Matters from a Dark First-Order Phase Transition,” [arXiv:1911.12342 \[hep-ph\]](#).
- [34] D. Croon, T. E. Gonzalo, and G. White, “Gravitational Waves from a Pati-Salam Phase Transition,” [arXiv:1812.02747 \[hep-ph\]](#).
- [35] A. Greljo, T. Opferkuch, and B. A. Stefanek, “Gravitational Imprints of Flavor Hierarchies,” *Phys. Rev. Lett.* **124** no. 17, (2020) 171802, [arXiv:1910.02014 \[hep-ph\]](#).
- [36] W.-C. Huang, F. Sannino, and Z.-W. Wang, “Gravitational Waves from Pati-Salam Dynamics,” [arXiv:2004.02332 \[hep-ph\]](#).
- [37] V. Brdar, L. Graf, A. J. Helmboldt, and X.-J. Xu, “Gravitational Waves as a Probe of Left-Right Symmetry Breaking,” *JCAP* **12** (2019) 027, [arXiv:1909.02018 \[hep-ph\]](#).
- [38] M. Hindmarsh, S. J. Huber, K. Rummukainen, and D. J. Weir, “Gravitational waves from the sound of a first order phase transition,” *Phys. Rev. Lett.* **112** (2014) 041301, [arXiv:1304.2433 \[hep-ph\]](#).
- [39] M. Hindmarsh, S. J. Huber, K. Rummukainen, and D. J. Weir, “Numerical simulations of acoustically generated gravitational waves at a first order phase transition,” *Phys. Rev. D* **92** no. 12, (2015) 123009, [arXiv:1504.03291 \[astro-ph.CO\]](#).
- [40] M. Hindmarsh, S. J. Huber, K. Rummukainen, and D. J. Weir, “Shape of the acoustic gravitational wave power spectrum from a first order phase transition,” *Phys. Rev. D* **96** no. 10, (2017) 103520, [arXiv:1704.05871 \[astro-ph.CO\]](#).



- [41] J. R. Espinosa, T. Konstandin, J. M. No, and G. Servant, “Energy Budget of Cosmological First-order Phase Transitions,” *JCAP* **1006** (2010) 028, [arXiv:1004.4187 \[hep-ph\]](#).
- [42] M. Hindmarsh, “Sound shell model for acoustic gravitational wave production at a first-order phase transition in the early Universe,” *Phys. Rev. Lett.* **120** no. 7, (2018) 071301, [arXiv:1608.04735 \[astro-ph.CO\]](#).
- [43] M. Hindmarsh and M. Hijazi, “Gravitational waves from first order cosmological phase transitions in the Sound Shell Model,” *JCAP* **1912** no. 12, (2019) 062, [arXiv:1909.10040 \[astro-ph.CO\]](#).
- [44] G. Kane, K. Sinha, and S. Watson, “Cosmological Moduli and the Post-Inflationary Universe: A Critical Review,” *Int. J. Mod. Phys. D* **24** no. 08, (2015) 1530022, [arXiv:1502.07746 \[hep-th\]](#).
- [45] R. Allahverdi *et al.*, “The First Three Seconds: a Review of Possible Expansion Histories of the Early Universe,” [arXiv:2006.16182 \[astro-ph.CO\]](#).
- [46] T. Banks, M. Berkooz, S. Shenker, G. W. Moore, and P. Steinhardt, “Modular cosmology,” *Phys. Rev. D* **52** (1995) 3548–3562, [arXiv:hep-th/9503114](#).
- [47] T. Banks, M. Berkooz, and P. Steinhardt, “The Cosmological moduli problem, supersymmetry breaking, and stability in postinflationary cosmology,” *Phys. Rev. D* **52** (1995) 705–716, [arXiv:hep-th/9501053](#).
- [48] G. Coughlan, W. Fischler, E. W. Kolb, S. Raby, and G. G. Ross, “Cosmological Problems for the Polonyi Potential,” *Phys. Lett. B* **131** (1983) 59–64.
- [49] T. Banks, D. B. Kaplan, and A. E. Nelson, “Cosmological implications of dynamical supersymmetry breaking,” *Phys. Rev. D* **49** (1994) 779–787, [arXiv:hep-ph/9308292](#).
- [50] B. Dutta, L. Leblond, and K. Sinha, “Mirage in the Sky: Non-thermal Dark Matter, Gravitino Problem, and Cosmic Ray Anomalies,” *Phys. Rev. D* **80** (2009) 035014, [arXiv:0904.3773 \[hep-ph\]](#).
- [51] R. Allahverdi, B. Dutta, and K. Sinha, “Successful Supersymmetric Dark Matter with Thermal Over/Under-Abundance from Late Decay of a Visible Sector Scalar,” *Phys. Rev. D* **87** (2013) 075024, [arXiv:1212.6948 \[hep-ph\]](#).
- [52] B. S. Acharya, P. Kumar, K. Bobkov, G. Kane, J. Shao, and S. Watson, “Non-thermal Dark Matter and the Moduli Problem in String Frameworks,” *JHEP* **06** (2008) 064, [arXiv:0804.0863 \[hep-ph\]](#).
- [53] B. S. Acharya, G. Kane, S. Watson, and P. Kumar, “A Non-thermal WIMP Miracle,” *Phys. Rev. D* **80** (2009) 083529, [arXiv:0908.2430 \[astro-ph.CO\]](#).
- [54] A. L. Erickcek, K. Sinha, and S. Watson, “Bringing Isolated Dark Matter Out of Isolation: Late-time Reheating and Indirect Detection,” *Phys. Rev. D* **94** no. 6, (2016) 063502, [arXiv:1510.04291 \[hep-ph\]](#).
- [55] M. Sten Delos, T. Linden, and A. L. Erickcek, “Breaking a dark degeneracy: The gamma-ray signature of early matter domination,” *Phys. Rev. D* **100** no. 12, (2019) 123546, [arXiv:1910.08553 \[astro-ph.CO\]](#).
- [56] A. L. Erickcek, “The Dark Matter Annihilation Boost from Low-Temperature Reheating,” *Phys. Rev. D* **92** no. 10, (2015) 103505, [arXiv:1504.03335 \[astro-ph.CO\]](#).
- [57] M. Drees and F. Hajkarim, “Dark Matter Production in an Early Matter Dominated Era,” *JCAP* **02** (2018) 057, [arXiv:1711.05007 \[hep-ph\]](#).
- [58] C. Cosme, M. Dutra, T. Ma, Y. Wu, and L. Yang, “Neutrino Portal to FIMP Dark Matter with an Early Matter Era,” [arXiv:2003.01723 \[hep-ph\]](#).
- [59] R. Allahverdi, B. Dutta, and K. Sinha, “Baryogenesis and Late-Decaying Moduli,” *Phys. Rev. D* **82** (2010) 035004, [arXiv:1005.2804 \[hep-ph\]](#).
- [60] C. Pallis, “Kination-dominated reheating and cold dark matter abundance,” *Nucl. Phys. B* **751** (2006) 129–159, [arXiv:hep-ph/0510234](#).

- [61] J. Lankinen, O. Kerppo, and I. Vilja, “Reheating via gravitational particle production in the kination epoch,” *Phys. Rev. D* **101** no. 6, (2020) 063529, [arXiv:1910.07520 \[gr-qc\]](#).
- [62] K. Nakayama and F. Takahashi, “Running Kinetic Inflation,” *JCAP* **11** (2010) 009, [arXiv:1008.2956 \[hep-ph\]](#).
- [63] C. Pallis, “Quintessential kination and cold dark matter abundance,” *JCAP* **10** (2005) 015, [arXiv:hep-ph/0503080](#).
- [64] D. Grin, T. L. Smith, and M. Kamionkowski, “Axion constraints in non-standard thermal histories,” *Phys. Rev. D* **77** (2008) 085020, [arXiv:0711.1352 \[astro-ph\]](#).
- [65] K. Dimopoulos and T. Markkanen, “Non-minimal gravitational reheating during kination,” *JCAP* **06** (2018) 021, [arXiv:1803.07399 \[gr-qc\]](#).
- [66] K. Redmond and A. L. Erickcek, “New Constraints on Dark Matter Production during Kination,” *Phys. Rev. D* **96** no. 4, (2017) 043511, [arXiv:1704.01056 \[hep-ph\]](#).
- [67] G. Barenboim and W.-I. Park, “Gravitational waves from first order phase transitions as a probe of an early matter domination era and its inverse problem,” *Phys. Lett.* **B759** (2016) 430–438, [arXiv:1605.03781 \[astro-ph.CO\]](#).
- [68] N. Bernal and F. Hajkarim, “Primordial Gravitational Waves in Nonstandard Cosmologies,” *Phys. Rev. D* **100** no. 6, (2019) 063502, [arXiv:1905.10410 \[astro-ph.CO\]](#).
- [69] C. Caprini and D. G. Figueroa, “Cosmological Backgrounds of Gravitational Waves,” *Class. Quant. Grav.* **35** no. 16, (2018) 163001, [arXiv:1801.04268 \[astro-ph.CO\]](#).
- [70] F. D’Eramo and K. Schmitz, “Imprint of a scalar era on the primordial spectrum of gravitational waves,” *Phys. Rev. Research*. **1** (2019) 013010, [arXiv:1904.07870 \[hep-ph\]](#).
- [71] M. Geller, A. Hook, R. Sundrum, and Y. Tsai, “Primordial Anisotropies in the Gravitational Wave Background from Cosmological Phase Transitions,” *Phys. Rev. Lett.* **121** no. 20, (2018) 201303, [arXiv:1803.10780 \[hep-ph\]](#).
- [72] Y. Cui, M. Lewicki, D. E. Morrissey, and J. D. Wells, “Cosmic Archaeology with Gravitational Waves from Cosmic Strings,” *Phys. Rev. D* **97** no. 12, (2018) 123505, [arXiv:1711.03104 \[hep-ph\]](#).
- [73] J. Ellis, M. Lewicki, and J. M. No, “On the Maximal Strength of a First-Order Electroweak Phase Transition and its Gravitational Wave Signal,” *Submitted to: JCAP* (2018) , [arXiv:1809.08242 \[hep-ph\]](#).
- [74] J. Ellis, M. Lewicki, and J. M. No, “Gravitational waves from first-order cosmological phase transitions: lifetime of the sound wave source,” [arXiv:2003.07360 \[hep-ph\]](#).
- [75] S. Weinberg, *Cosmology*. 9, 2008.
- [76] A. D. Linde, “Fate of the False Vacuum at Finite Temperature: Theory and Applications,” *Phys. Lett.* **100B** (1981) 37–40.
- [77] A. D. Linde, “Decay of the False Vacuum at Finite Temperature,” *Nucl. Phys.* **B216** (1983) 421. [Erratum: *Nucl. Phys.* **B223**,544(1983)].
- [78] G. V. Dunne and H. Min, “Beyond the thin-wall approximation: Precise numerical computation of prefactors in false vacuum decay,” *Phys. Rev. D* **72** (2005) 125004, [arXiv:hep-th/0511156 \[hep-th\]](#).
- [79] A. Andreassen, D. Farhi, W. Frost, and M. D. Schwartz, “Precision decay rate calculations in quantum field theory,” *Phys. Rev. D* **95** no. 8, (2017) 085011, [arXiv:1604.06090 \[hep-th\]](#).
- [80] S. Weinberg, *The quantum theory of fields. Vol. 2: Modern applications*. Cambridge University Press, 2013.
- [81] R. J. Scherrer and M. S. Turner, “Decaying Particles Do Not Heat Up the Universe,” *Phys. Rev. D* **31** (1985) 681.

- [82] A. H. Guth and E. J. Weinberg, “Cosmological Consequences of a First Order Phase Transition in the SU(5) Grand Unified Model,” *Phys. Rev.* **D23** (1981) 876.
- [83] G. D. Moore and T. Prokopec, “How fast can the wall move? A Study of the electroweak phase transition dynamics,” *Phys. Rev.* **D52** (1995) 7182–7204, [arXiv:hep-ph/9506475 \[hep-ph\]](#).
- [84] R. Apreda, M. Maggiore, A. Nicolis, and A. Riotto, “Gravitational waves from electroweak phase transitions,” *Nucl. Phys.* **B631** (2002) 342–368, [arXiv:gr-qc/0107033 \[gr-qc\]](#).
- [85] R.-G. Cai and S.-J. Wang, “Energy budget of cosmological first-order phase transition in FLRW background,” *Sci. China Phys. Mech. Astron.* **61** (2018) 080411, [arXiv:1803.03002 \[gr-qc\]](#).
- [86] J. Ignatius, K. Kajantie, H. Kurki-Suonio, and M. Laine, “The growth of bubbles in cosmological phase transitions,” *Phys. Rev. D* **49** (1994) 3854–3868, [arXiv:astro-ph/9309059](#).
- [87] H. Kurki-Suonio and M. Laine, “On bubble growth and droplet decay in cosmological phase transitions,” *Phys. Rev. D* **54** (1996) 7163–7171, [arXiv:hep-ph/9512202](#).
- [88] B.-H. Liu, L. D. McLerran, and N. Turok, “Bubble nucleation and growth at a baryon number producing electroweak phase transition,” *Phys. Rev.* **D46** (1992) 2668–2688.
- [89] D. Cutting, M. Hindmarsh, and D. J. Weir, “Vorticity, kinetic energy, and suppressed gravitational wave production in strong first order phase transitions,” [arXiv:1906.00480 \[hep-ph\]](#).
- [90] T. Konstandin, G. Nardini, and I. Rues, “From Boltzmann equations to steady wall velocities,” *JCAP* **1409** no. 09, (2014) 028, [arXiv:1407.3132 \[hep-ph\]](#).
- [91] A. Brandenburg, K. Enqvist, and P. Olesen, “Large scale magnetic fields from hydromagnetic turbulence in the very early universe,” *Phys. Rev.* **D54** (1996) 1291–1300, [arXiv:astro-ph/9602031 \[astro-ph\]](#).
- [92] R. M. Gailis, N. E. Frankel, and C. P. Dettmann, “Magnetohydrodynamics in the expanding Universe,” *Phys. Rev.* **D52** no. 12, (1995) 6901.
- [93] H. Kurki-Suonio and M. Laine, “Supersonic deflagrations in cosmological phase transitions,” *Phys. Rev.* **D51** (1995) 5431–5437, [arXiv:hep-ph/9501216 \[hep-ph\]](#).
- [94] U.-L. Pen and N. Turok, “Shocks in the Early Universe,” *Phys. Rev. Lett.* **117** no. 13, (2016) 131301, [arXiv:1510.02985 \[astro-ph.CO\]](#).
- [95] M. Dine, R. G. Leigh, P. Y. Huet, A. D. Linde, and D. A. Linde, “Towards the theory of the electroweak phase transition,” *Phys. Rev. D* **46** (1992) 550–571, [arXiv:hep-ph/9203203](#).
- [96] C. L. Wainwright, “CosmoTransitions: Computing Cosmological Phase Transition Temperatures and Bubble Profiles with Multiple Fields,” *Comput. Phys. Commun.* **183** (2012) 2006–2013, [arXiv:1109.4189 \[hep-ph\]](#).
- [97] P. Athron, C. Balzs, M. Bardsley, A. Fowlie, D. Harries, and G. White, “BubbleProfiler: finding the field profile and action for cosmological phase transitions,” [arXiv:1901.03714 \[hep-ph\]](#).